Quantum Simulations with Unitary and Nonunitary Controls: NMR implementations

A thesis
Submitted in partial fulfillment of the requirements
Of the degree of
Doctor of Philosophy

By

Swathi S Hegde
20103089

INDIAN INSTITUTE OF SCIENCE EDUCATION AND RESEARCH PUNE

May, 2016

Certificate

Certified that the work incorporated in the thesis entitled "*Quantum Simulations with Unitary and Nonunitary Controls: NMR implementations*", submitted by *Swathi S Hegde* was carried out by the candidate, under my supervision. The work presented here or any part of it has not been included in any other thesis submitted previously for the award of any degree or diploma from any other University or institution.

Date **Dr. T. S. Mahesh**

Declaration

I declare that this written submission represents my ideas in my own words and where others' ideas have been included, I have adequately cited and referenced the original sources. I also declare that I have adhered to all principles of academic honesty and integrity and have not misrepresented or fabricated or falsified any idea/data/fact/source in my submission. I understand that violation of the above will be cause for disciplinary action by the Institute and can also evoke penal action from the sources which have thus not been properly cited or from whom proper permission has not been taken when needed.

Date **Swathi S Hegde**

Roll No.- 20103089

Acknowledgement

Publications

1. Ravi Shankar, Swathi S. Hegde, and T. S. Mahesh,
   Quantum simulations of a particle in one- dimensional potentials using NMR,
   Physics Letters A 378, 10 (2014).

2. Swathi S. Hegde and T. S. Mahesh,
   Engineered Decoherence: Characterization and Suppression,
   Phys. Rev. A 89, 062317 (2014).

3. Swathi S. Hegde, Hemant Katiyar, T. S. Mahesh, and Arnab Das,
   Freezing a Quantum Magnet by Repeated Quantum Interference: An Experimental Realization,
   Phys. Rev. B 90, 174407(2014).

4. T. S. Mahesh, Abhishek Shukla, Swathi S. Hegde, C. S. Sudheer Kumar, Hemant Katiyar, Sharad Joshi, and K. R. Koteswara Rao,
   Ancilla assisted measurements on quantum ensembles: General protocols and applications in NMR quantum information processing,
   Current Science, 109, 1987 (2015).

5. Anjusha V. S., Swathi S. Hegde, and T. S. Mahesh,
   NMR simulation of the Quantum Pigeonhole Effect,
   Phys. Lett. A, 380, 577 (2016).

6. Swathi S. Hegde, K. R. Koteswara Rao, and T. S. Mahesh,

Pauli Decomposition over Commuting Subsets: Applications in Gate Synthesis, State Preparation, and Quantum Simulations,
arXiv:1603.06867 (2016).

Contents

List of Figures

Chapter 1

Quantum simulation

> *"Nature isn't classical, dammit, and if you want to make a simulation of nature, you'd better make it quantum mechanical, and by golly it's a wonderful problem, because it doesn't look so easy".*
>
> *- Richard Feynman, 1982 [1].*

1.1 Introduction

The origin of the quantum physics dates back to the year 1900 when Max Planck tried to give an explanation for the properties of the black-body radiation [2]. This quantum theory was further developed by Schrödinger, Dirac and other eminent physicists leading to the understanding of quantum mechanics as we now know [3, 4, 5]. More than a century since its inception, we still believe that quantum mechanics is the correct description of the present understanding of nature. Yet this subject is so counter-intuitive that it has never ceased to surprise us even now.

Quantum mechanics has a lot of applications in the present day science and technology. For example, it is an indispensable tool to understand the structure of atoms, molecules and their interactions; the invention of magnetic resonance imaging has revolutionized the field of medicine; lasers are heavily used in medicine, communication, industries, etc; and the list goes on. This thesis deals with one other application of quantum physics, i.e, quantum information processing (QIP) and quantum computation (QC).

Quantum computers are believed to be capable of solving certain physical and mathematical problems much more efficiently than the classical computers [6, 7, 8]. The phenomenon of quantum superposition offers computational parallelism that is beyond the classical paradigm hence rendering quantum processors more efficient.

Coupled quantum particles that can be precisely addressed, controlled and measured form the basic hardware of a quantum computer. Moreover, in order to implement quantum computation, Di Vincenzo gave certain criteria that the quantum computer should posses [9]. These requirements are as follows:

1. Scalable and well defined quantum system.
2. Ability to initialize the quantum system to a desired initial state.
3. Long coherence times so as to implement specific gate operations.
4. A set of quantum gates which are universal.
5. Ability to perform a qubit-specific measurement.

One important application of quantum computers is to simulate quantum mechanical systems and this field of quantum simulations is the primary subject of this thesis. Owing to a huge memory requirement, simulating quantum mechanics using a classical computer is a challenging problem. The memory amounts to the storage of the probability amplitudes of the state of the quantum systems and grows exponentially with the number (n) of the quantum systems [10] (see section. 2.1.2). For example, for a 2-level quantum system, also known as a quantum bit or a *qubit*, and for $n = 40$, a classical computer has to store 2^{40}

parameters and hence the problem becomes intractable. As a possible solution to this limitation, Feynman in 1982 [1], proposed the concept of quantum simulator to perform quantum simulations:

> *"Let the computer itself be built of quantum mechanical elements which obey quantum mechanical laws."*

A quantum simulator is basically a quantum computer that can mimic the dynamics of other quantum systems we wish to study. The idea is to realize the dynamics of a quantum system using other accessible and controllable quantum systems. By doing so, the Hilbert space of the quantum simulator is thus capable of storing 2^n complex amplitudes using only n (or $\propto n$) qubits.

A typical quantum simulation protocol is explained in Fig. 1.1 [11]. The upper box represents the dynamics of a quantum system that we wish to study. Here the quantum system in the initial state $|\phi(0)\rangle$ evolves to a final state $|\phi(t)\rangle$ under the action of an operator U. The lower box corresponds to the quantum simulator that is used to simulate the above evolution. The way to implement

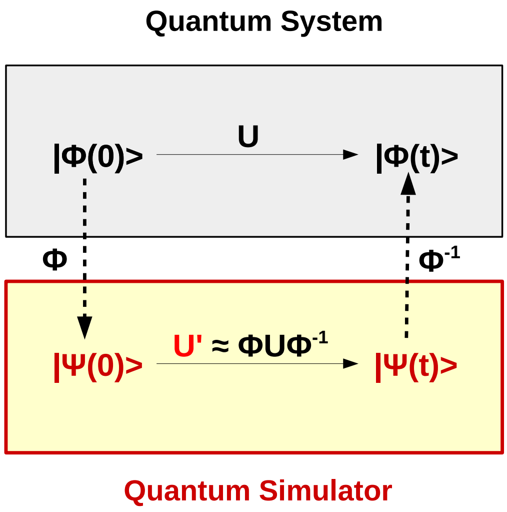

Figure 1.1: Quantum simulation protocol.

quantum simulation is by encoding $|\phi(0)\rangle$ into the initial state $|\psi(0)\rangle$ of the quantum simulator followed by the application of U'. The operator U' has a one-to-one correspondence with U and is related by the transformation $U' = \phi U \phi^{-1}$, where ϕ is a linear map. The final state $|\psi(t)\rangle$ of the quantum simulator encodes the information corresponding to $|\phi(t)\rangle$.

1.2 Thesis structure

Fig. 1.2 gives the pictorial representation of the thesis structure.

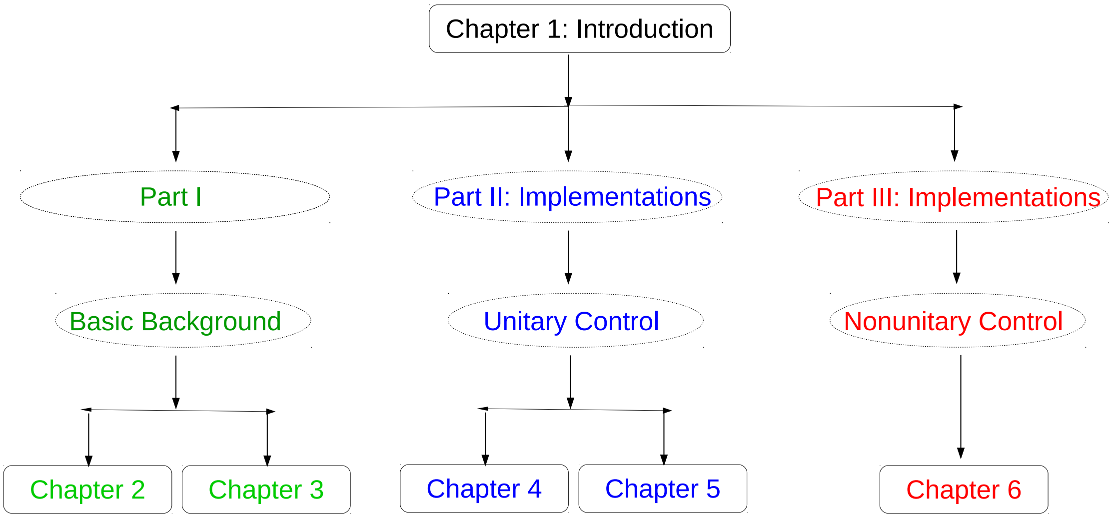

Figure 1.2: Structure of the thesis.

The thesis contains three parts.

- The first part consists of chapter 2 and chapter 3. Chapter 2 deals with the basic terminology and theory of quantum information processing. It includes the description of quantum states, their evolution and measurement schemes that forms the platform to understand a quantum simulation protocol as mentioned in the previous section. Chapter 3 explains the basics of nuclear magnetic resonance (NMR) and how nuclear spins in NMR can be used as quantum simulators.

- The second part is about the implementations of quantum simulations using unitary control. It consists of two related works and are explained in chapters 4 and 5.
- Finally, part III deals with the implementations of non-unitary dynamics and the related work is explained in chapter 6.

Three different works [12, 13, 14] that form the backbone of this thesis are explained in detail in chapters 4 to 6. A brief description of these three chapters are given in the section 1.3.

1.3 Implementations

Since a couple of decades various quantum devices are believed to be promising candidates for quantum simulations. Among them are the nuclear spins [15, 16], electron spins in quantum dots [17], neutral atoms [18], trapped ions [19], superconducting circuits [20], etc, each with strengths and challenges as shown in table 1.1. As of now, the number of quantum simulation experiments that are done or are proposed to be implemented is almost exhaustive [21, 22, 23, 24, 25, 26, 27, 28, 29]. However, large-scale quantum simulators are yet to become a reality. The main obstacles for this are the scalability, precise control of the dynamics and decoherence.

In this thesis I will explain some aspects of quantum simulations using both unitary and nonunitary controls. Specifically, we address the problems of quantum control and decoherence. While we use nuclear spin 1/2 systems in an NMR setup as our quantum simulators, most of the concepts are general and are applicable elsewhere. The experimental implementations of these aspects that are a part of thesis are briefly explained below:

Quantum simulators	Strength	Challenges
Nuclear spins	Well established, readily available technology	Scaling, individual control
Electron spins	Individual control, readout	Scaling
Neutral atoms	Scaling	Individual control, readout
Trapped ions	Individual control, readout	Scaling
Superconducting circuits	Individual control, readout	Scaling

Table 1.1: Strenght and challenges of a few quantum simulators [10].

1. Chapter 4 describes unitary control, the methodology, and one particular quantum simulation realized using the advanced optimal quantum control techniques. I will first describe the novel quantum phenomenon known as "quantum exotic freezing", proposed by Arnab Das in 2010 [30]. It is based on dynamical quantum many-body localization, wherein a spin-chain freezes its dynamics for certain specific frequencies of external drive. Unlike classical systems, the quantum systems freeze and respond non-monotonically with the frequency of the external drive. Here I will describe the first experimental observation of quantum exotic freezing using an NMR system consisting of three mutually interacting spin 1/2 nuclei [12]. I will also describe the importance of robust unitary control over spin-dynamics. Particularly, I will describe the implementation of GRadient Ascent Pulse Engineering (GRAPE) protocol for robust unitary control.

2. Chapter 5 addresses the problem of decomposition of an arbitrary unitary operator in terms of simpler unitaries. Here we propose a general numerical algorithm, namely Pauli Decomposition over Commuting Subsets (PDCS), to decompose an arbitrary unitary operator in terms of simpler *rotors* [13]. Each rotor is expressed as a generalized rotation over a mutually commuting set of Pauli operators. Using PDCS, we decomposed several quantum gates and circuits and also showed its application in designing quantum circuits for state preparation. We hypothesize the decomposition

method to scale efficiently with the size of the system, and propose its application in quantum simulations. As an example, I will describe quantum simulation of three-body interaction using a three-spin NMR system and monitor the dynamics with the help of overall magnetization.

3. In practice, quantum systems are affected by their interactions with the environment leading to an undesirable nonunitary process known as decoherence. This process is accompanied by the loss of information in the quantum processors and is a major obstacle in experimental quantum information processing and computation. One of the ways to fight this process is to understand decoherence. Teklemariam *et al.*, in 2003 [31], described a way of introducing the artificial decoherence on a quantum system by randomly perturbing an ancillary system. Recently, in a different context, Alvarez *et al.* and Yuge *et al.*, have independently proposed noise spectroscopy to characterize the noise acting on a quantum system [32, 33]. In Chapter 6, I will describe the experimental implementation of such an engineered noise introduced by random RF pulses on an ancillary spin using an NMR spin-system. I will also describe the characterization of the engineered noise by both noise spectroscopy and quantum process tomography. Further, we supressed this induced noise using dynamical decoupling (DD) which is a process of suppression of decoherence by systematic modulation of system state. Chapter 6 also describes the first experimental study of competition between the engineered decoherence and DD [14].

Part I

Basic Background

Chapter 2

Quantum information processing

This chapter gives a brief introduction to the theory of quantum information processing with a goal to provide a few useful techniques for implementing quantum simulations. A typical quantum computation algorithm consists of an input, processing and an output. Below is a brief summary of these three major steps:

1. State initialization: A *quantum state* $|\psi(t)\rangle$ contains the entire description of the quantum system. As an input of any quantum algorithm, it is required that any given quantum system is initialized to a known state $|\psi(0)\rangle$.

2. Gate implementation: Processing of the information is done using quantum gates. A quantum gate is realized by the *unitary operator* $U(t)$ that evolves the initial state $|\psi(0)\rangle$ to the final state $|\psi(t)\rangle$.

3. Measurements: The final state $|\psi(t)\rangle$ or the expectation value of any hermitian operators $\hat{A}$ in the state $|\psi(t)\rangle$ that encodes the solution to the algorithm is obtained by a *measurement* process.

With reference to the above steps, this chapter concentrates on the theory of state description, gate operation and measurements. For extensive details about these topics it is reccommended to refer to [6, 7].

2.1 Quantum States

This section explains the basic terminology and properties of the quantum states.

2.1.1 Single qubit

A qubit is a quantum counterpart of a classical bit. Physically, any two level quantum system is a qubit. Mathematically, the most general state of a qubit is represented as

$$|\psi\rangle = \alpha|0\rangle + \beta|1\rangle, \tag{2.1}$$

where α, β are the probability amplitudes with $|\alpha|^2 + |\beta|^2 = 1$, and $|0\rangle$, $|1\rangle$ are the orthogonal states and form a computational basis.

The geometric representation of a single qubit state (Eq. 2.1) is visualized by Bloch sphere as shown in Fig. 2.1. Here $\alpha = \cos(\frac{\theta}{2})$ and $\beta = e^{i\phi}\sin(\frac{\theta}{2})$ where $\theta = [0, \pi]$ and $\phi = [0, 2\pi]$ are the points on the unit sphere. The state $|\psi\rangle$ can exist anywhere in the sphere.

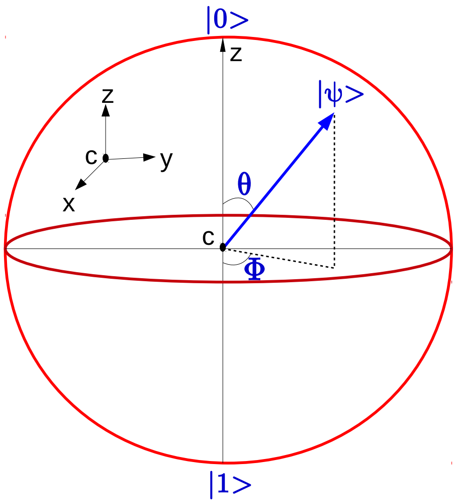

Figure 2.1: Bloch sphere representation of $|\psi\rangle$.

Thus as seen from Eq. 2.1, a qubit can exist in a linear superposition of $|0\rangle$

and $|1\rangle$. The complex numbers α and β have the information of the basis states and thus a qubit can store 2 bits of information until measured. This is in contrast with the classical bits which can be either 0 or 1 and can have only one bit of information at a time. This property of superposition enables quantum parallelism that renders quantum computers more powerful than classical computers in terms of the computational speed and storage capacity.

2.1.2 Multiple qubits

As discussed in section 1.1, a typical quantum computer requires mutiple interacting qubits. Apart from the phenomenon of quantum superposition, such quantum systems exhibit one of the most powerful properties called entanglement.

Suppose there are two qubits described by the states $|\psi_1\rangle = \alpha_1|0\rangle + \beta_1|1\rangle$ and $|\psi_2\rangle = \alpha_2|0\rangle + \beta_2|1\rangle$ where $|\alpha_1|^2 + |\beta_1|^2 = 1$ and $|\alpha_2|^2 + |\beta_2|^2 = 1$. The state of the composite system is represented by

$$|\psi\rangle = |\psi_1\rangle \otimes |\psi_2\rangle = |\psi_1\rangle|\psi_2\rangle, \tag{2.2}$$

where $\otimes$ is the tensor product. Hence $|\psi\rangle = \alpha_1\alpha_2|00\rangle + \alpha_1\beta_2|01\rangle + \beta_1\alpha_2|10\rangle + \beta_1\beta_2|11\rangle$ with $|\alpha_1\alpha_2|^2 + |\alpha_1\beta_2|^2 + |\beta_1\alpha_2|^2 + |\beta_1\beta_2|^2 = 1$ and is described by $2^2 = 4$ complex numbers. The states $\{|00\rangle, |01\rangle, |10\rangle, |11\rangle\}$ form the computational basis of this two qubit system.

In a similar way, an n-qubit system is represented by the state

$$|\psi\rangle^{\otimes n} = |\psi_1\rangle|\psi_2\rangle \cdots |\psi_n\rangle, \tag{2.3}$$

One can observe that a total of 2^n basis states is required to describe an n-qubit state. Thus in order to describe an n-qubit state, one requires 2^n probability amplitudes indicating an exponential growth with the n.

2.1.3 Density operator formalism

Quantum state for an ensemble of quantum systems is generally described by using the density operators [34]. In this section, I will introduce to the density operator formalism.

2.1.3.1 Density operator

A density operator of an n-qubit system is defined as

$$\rho = \sum_{i}^{n} p_i |\psi_i\rangle\langle\psi_i|, \tag{2.4}$$

where $|\psi_i\rangle$ is the state of the i^{th} sub-system and p_i's are the corresponding probabilities such that $\sum_i^n p_i = 1$.

Another description of a single qubit density operator expressed in Pauli operator basis is given by

$$\rho = \frac{1}{2}(\mathbb{I} + r \cdot \sigma), \tag{2.5}$$

where $\mathbb{I}$ is the Identity operator, r is the 3-dimentional unit vector and $\sigma \in \{X, Y, Z\}$ are the Pauli operators defined by:

$$X = \begin{bmatrix} 0 & 1 \\ 1 & 0 \end{bmatrix}; \qquad Y = \begin{bmatrix} 0 & -i \\ i & 0 \end{bmatrix}; \qquad Z = \begin{bmatrix} 1 & 0 \\ 0 & -1 \end{bmatrix}; \tag{2.6}$$

Also, in the matrix representation

$$\rho = \begin{pmatrix} \rho_{00} & \rho_{01} \\ \rho_{10} & \rho_{11} \end{pmatrix}. \tag{2.7}$$

It is important to note that the diagonal elements ρ_{00}, ρ_{11} correspond to the populations and the off-diagonal elements ρ_{01}, ρ_{10} correspond to the coherences of the state. It should be noted that the populations add up to one and $\rho_{01} = \rho_{10}^{\dagger}$

since ρ is hermitian.

One can also express the density operator of the composite system as $\rho = \rho_1 \otimes \rho_2 \otimes \cdots \otimes \rho_n$.

Most importantly, any operator ρ should satisfy the following properties:

- $\mathrm{tr}(\rho) = 1$.
- ρ should be a positive operator (i.e., it should have non-negative eigen values).
- ρ should be hermitian. i.e., $\forall A, A = \tilde{A}^*$.

2.1.3.2 Reduced density operator

A reduced density operator describes the state of the sub-system when the density operator of the composite system is known.

Suppose the composite system is in the state ρ_{12} which contains two sub-systems namely 1 and 2. Then the sub-system states are given by

$$\rho_1 = \mathrm{tr}_2(\rho_{12}), \tag{2.8}$$

$$\rho_2 = \mathrm{tr}_1(\rho_{12}), \tag{2.9}$$

where the operation tr$_i$, with $i = 1, 2$, is called as partial trace. For example, the partial trace over the sub-system 2, i.e., ρ_2, is defined as

$$\rho_2 = \mathrm{tr}_1(\rho_{12}) = \mathrm{tr}_2(|\psi_1\rangle\langle\psi_1| \otimes |\psi_2\rangle\langle\psi_2|) = |\psi_1\rangle\langle\psi_1|\mathrm{tr}(|\psi_2\rangle\langle\psi_2|) = |\psi_1\rangle\langle\psi_1|\langle\psi_2|\psi_2\rangle.$$

2.1.3.3 State types

A state can be either pure, mixed, separable or entangled.

When all the sub-systems are in the same state $|\psi\rangle$, the composite system is known to be in pure state. It is required that the individual sub-systems in Eq. 2.4 are pure but the composite system may not always be pure. When different sub-systems have different states, the composite system is known to be in a mixed state. The condition for the composite state ρ to be either pure or mixed is defined as follows:

- Pure state: $\mathrm{tr}(\rho^2) = 1$.
- Mixed state: $\mathrm{tr}(\rho^2) < 1$.

Geometrically, the states on the surface of the bloch sphere of Fig. 2.1 are pure states and any other states inside the surface of the bloch sphere correspond to the mixed states.

An interesting consequence of ensemble quantum systems is the property of entanglement. If an n-qubit density matrix is expressed as

$$\rho = \rho_1 \otimes \rho_2 \otimes \cdots \otimes \rho_n, \tag{2.10}$$

then such a state is known to be seperable state. And if

$$\rho \neq \rho_1 \otimes \rho_2 \otimes \cdots \otimes \rho_n, \tag{2.11}$$

then such a state is known as entangled state.

It should be noted that suppose the composite system is described by a seperable state then its reduced density operator will be a pure state and if the composite system is described by an entangled state then its reduced density operator will be a mixed state.

2.2 Quantum gates

A quantum gate is an operation that evolves the quantum state from a specific initial state to a final state.

2.2.1 State evolution

Any closed quantum system with initial state $|\psi(0)\rangle$ evolves under a time dependent Hamiltonan $\mathcal{H}(t)$ according to

$$|\psi(t)\rangle = U(t)|\psi(0)\rangle, \tag{2.12}$$

where $U(t) = \mathcal{T}e^{\int_0^t -i\mathcal{H}(t')dt'}$ is a unitary operator. Here $\hbar$ is set to unity and $\mathcal{T}$ is the time ordering operator

Similarly, the evolution of the state in terms of $n-$qubit density operator $\rho(0)$ is obtained by combining equations 2.4 and 2.12 and is described as

$$\rho(t) = \sum_i^n p_i[U(t)|\psi_i(0)\rangle][\langle\psi_i(0)|U^\dagger]$$

$$\rho(t) = U(t)\rho(0)U(t)^\dagger \tag{2.13}$$

One of the main features of unitary operators is that they preserve the probabilities and coherence of the quantum states over time. In other words, unitarity imposes reversibility criteria which means that one should be able to get back the initial state $\rho(0)$ starting from $\rho(t)$:

$$U(t)^\dagger\rho(t)U(t) = U(t)^\dagger[U(t)\rho(0)U(t)^\dagger]U(t) = \rho(0),$$

since $UU^\dagger = U^\dagger U = \mathbb{I}$.

In the language of quantum computation, a unitary operator $U(t)$ corresponding to the transformation

$$\rho(0) \xrightarrow{U(t)} \rho(t)$$

is a quantum gate. Below, I will explain the quantum gates with reference to the circuit model of quantum computation.

2.2.2 Single qubit gates

Any unitary U transforms the quantum system from one state to another. Geometrically, U rotates any state vector $|\psi(0)\rangle$ to $|\psi(t)\rangle$ in the bloch sphere. Thus each single qubit U corresponds to a rotation about the axis $\hat{n}$ and is given by

$$R_{\hat{n}}^{\theta} = e^{-i\theta\hat{n}\cdot\vec{\sigma}/2} = \cos\left(\frac{\theta}{2}\right)\mathbb{I} - i\sin\left(\frac{\theta}{2}\right)(n_x X + n_y Y + n_z Z), \tag{2.14}$$

where $\hat{n} = \{n_x, n_y, n_z\}$ is the 3-dimensional unit vector and θ is the rotational angle.

Any single qubit operator can be contructed using Eq. 2.14. Some standard quantum gates like Hadamard (H) and phase gate (S) are listed below:

$$H = \frac{1}{\sqrt{2}}\begin{bmatrix} 1 & 1 \\ 1 & -1 \end{bmatrix}; \qquad S = \begin{bmatrix} 1 & 0 \\ 0 & i \end{bmatrix}; \tag{2.15}$$

Quantum operators with multiple non-commuting rotations should be carefully implemented in a specific time order. For convenience, the operators are acted from left to right in a quantum circuit. For example, as shown in Fig. 2.2, H corresponds to the rotation about X-axis with $\theta = 180°$ followed by a rotation about Y-axis with $\theta = 90°$. Thus, $H = R_y^{\pi/2} R_x^{\pi}$.

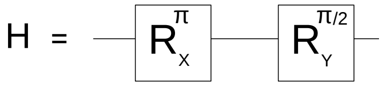

Figure 2.2: Single qubit Hadamard gate. Here the rotations are of the form of Eq. 2.14 and are implemented from left to right.

2.2.3 Two-qubit gates

A two qubit gate U_{12} exploits the knowlegde of single qubit gates as well as the interaction between the two qubits. Such gates play an important role in quantum computation as they can entangle the qubits. The circuit representation of U_{12} is shown in figure 2.3.

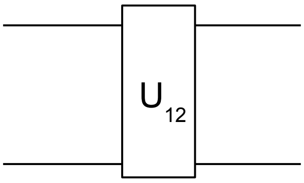

Figure 2.3: A general two qubit gate

A standard two qubit gate is a controlled-NOT (CNOT) gate represented by

$$U_{CNOT} = \begin{bmatrix} 1 & 0 & 0 & 0 \\ 0 & 1 & 0 & 0 \\ 0 & 0 & 0 & 1 \\ 0 & 0 & 1 & 0 \end{bmatrix} ; \qquad U_{CNOT}U_{CNOT}^{\dagger} = \mathbb{I}. \tag{2.16}$$

Figure 2.4 gives the circuit representation of U_{CNOT}. Qubit ① is the control and the qubit ② is the target with A and B as inputs. In convention, a filled circle indicates control and the cross indicates the target. The action of U_{CNOT} is

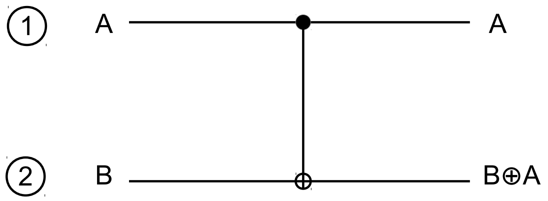

Figure 2.4: CNOT gate

written as

$$|A, B\rangle \longrightarrow |A, B \oplus A\rangle,$$

where $A, B \in \{0, 1\}$ and $\oplus$ is the addition modulo 2.

2.2.4 Universal gates

In order to realize arbitrary computation, one needs a universal set of gates. Just like a combination of NAND gates is universal in classical computation, there exists a set of quantum gates which are universal.

Any arbitrary single qubit gates along with CNOT gates form a universal set of quantum gates.

Specifically, one can consider Hadamard, phase gate, CNOT and $pi/8$ gates as a set of universal quantum gates. A more general observation is that any arbitrary single and two qubit gates can form universal quantum gates.

2.3 Measurements

Measurements are an important part of any algorithm and is a necessary step to extract any useful information. This step requires that the measuring device interacts with the quantum system, thus making the quantum system as an open quantum system. In general, measurments operations are nonunitary.

Suppose $\{M_m\}$ is the set of measurement operators that act on the state space of the system being measured. Here m is the measurement outcome of the operator that is measured. Let $|\psi\rangle$ be the state just before the measurement and the action of the measurement operators on $|\psi\rangle$ is defined as

$$|\psi\rangle' = \frac{M_m|\psi\rangle}{\sqrt{p}}, \tag{2.17}$$

where $|\psi\rangle'$ is the state after the measurement and $p = \langle\psi|M_m^\dagger M_m|\psi\rangle$ is the probability of obtaining the outcome m. Here $\sum_m p(m) = 1$, and $\sum_m M_m^\dagger M_m = \mathbb{I}$.

2.3.1 Projective measurements

Another class of measurements are projective measurements which is described by Hermitian operator M as

$$M = \sum_m m P_m, \tag{2.18}$$

where $P_m = |m\rangle\langle m|$ with $\{|m\rangle\}$ being the eigen states of M and m are its eigen values.

The probability of obtaining the outcome m after $|\psi\rangle$ is measured is given by

$$p(m) = \langle\psi|P_m|\psi\rangle, \tag{2.19}$$

and thus the measured state has the form

$$\frac{P_m|\psi\rangle}{\sqrt{p(m)}}. \tag{2.20}$$

Further it should be noted that for projective measurements, M_m should staisfy the following conditions:

- $\sum_m M_m^\dagger M_m = \mathbb{I}$
- $M_m M_m' = \delta_{m,m'} M_m$

Measurements are non-unitary operations. For example, the measurement operators for single qubit are $|0\rangle\langle 0|$ and $|1\rangle\langle 1|$. One can verify that each of these operators is Hermitian but is not unitary.

2.3.2 Ensemble average measurements

In many cases, one is intertested in obtaining the expectation value of an arbitrary operator A. The way to measure such an operator is to prepare a large number of quantum systems in the same initial states and the outcome corresponds to the probability weighted eigen values of A in some final state. It is definedS as follows:

$$\langle A(t)\rangle = \mathrm{Tr}[A(t)\rho(t)], \tag{2.21}$$

where $\rho(t)$ is the normalized final state. It is important that the operator A is hermitian since its eigen values are real. While the eigen values can take discrete values, the expectation values can take continuous values.

2.4 Quantum algorithms

2.5 Summary

Chapter 3

Liquid-state NMR quantum simulators

3.1 Nuclear magnetic resonance

When a quantum particle with non-zero nuclear spin angular momentum is placed in an external static magnetic field (B_0), there is an interaction between the particle and the field. This interaction leads to the splitting of the energy levels of the quantum particle, a phenomenon known as "Zeeman effect". Thus in the presence of B_0 along the $z-$axis, the splitting of the levels correspond to the following quantized energies:

$$E_m = -\mu_z B_0; \qquad \mu_z = \gamma \hbar m. \tag{3.1}$$

Here γ is the gyromagnetic ratio of the nuclei and the magnetic quantum number $m = [-I, -I+1, \cdots, I-1, I]$ takes $2I+1$ values where I is the nuclear spin quantum number.

The energy difference between the states m and $m+1$ can be obtained by calculating $\Delta E = E_{m+1} - E_m$ using Eq. 3.1 and the corresponding frequency

$\omega_0 = \Delta E/\hbar$ given by

$$\omega_0 = \gamma B_0. \tag{3.2}$$

This frequency is known as the *Larmor frequency* and plays a major role is addressing different nuclear spin species. A resonant absorption of energy is acheived when such an NMR active spin with definite ω_0 is perturbed by an external periodic field with same frequency as ω_0. This phenomenon is called as nuclear magnetic resonance (NMR).

Nuclei which exhibit this phenomenon are called as NMR active nuclei. Some common examples include ^{1}H,^{13}C,^{14}N,^{19}F, etc and their intrinsic properties are listed in table 3.1.

Nucleus	I	$\gamma\ (Ts)^{-1}$
^{1}H	1/2	2.6752×10^8
^{13}C	1/2	6.728×10^7
^{14}N	1	1.934×10^7
^{19}F	1/2	2.5181×10^8
^{31}P	1/2	1.0841×10^8

Table 3.1: NMR active nuclei and their intrinsic properties.

The rest of this thesis deals with nuclear spins corresponding to $I = 1/2$.

3.2 NMR qubits

3.2.1 Single qubit

A single spin-1/2 nuclei in a molecule placed in B_0 has a unique ω_0 and represents a qubit as shown in figure 3.1.

The internal Hamiltonian of such a single qubit system is given by

$$H_0 = \omega_0 I_z, \tag{3.3}$$

where the spin operator $I_z = \sigma_z/2$. The eigen states of H_0 are $|0\rangle$ and $|1\rangle$ with the energy difference given by $\hbar\omega_0$.

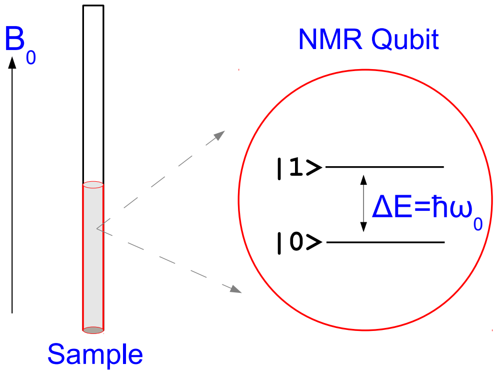

Figure 3.1: Zeeman splitting of a spin-1/2 nuclei.

A typical liquid state NMR sample consists of an avagadro number of molecules. The inter-molecular couplings are neglected by adding suitable solvents to the NMR sample. Despite this large number of molecules, an NMR active nuclei in each of the molecules has the same ω_0 and thus when viewed in frequency domain the entire sample is considered as a single qubit NMR system.

3.2.2 Multiple qubits

A molecule may contain multiple coupled spin-1/2 nuclei. The spins can be either of the same or different species and hence categorized as homonuclear or heteronuclear molecules respectively. In isotropic liquids state, the intermolecular and intramolecular dipolar couplings are averaged out due to the rapid motions of the molecules and thus only the scalar couplings that are mediated by the electrons in the intramolecular nuclear bonds are present. Thus the internal Hamiltonian for multiple qubits in the lab frame is given by

$$H_0 = \sum_{i=1}^{n} \omega_i I_z^i + 2\pi \sum_{i<j}^{n} J_{ij} I^i \cdot I^j, \tag{3.4}$$

where n is the number of qubits, J_{ij} are the scalar couplings and ω_i are the larmor frequencies.

If $|\omega_i - \omega_j| \ll 2\pi J_{ij}$ then the spins are strongly coupled else they are weakly coupled. Under the weak coupling limit, Eq. 3.4 reduces to

$$H_0 = \sum_{i=1}^{n} \omega_i I_z^i + 2\pi \sum_{i<j}^{n} J_{ij} I_z^i I_z^j. \tag{3.5}$$

3.3 State initialization

3.4 NMR gates

3.5 NMR measurements

Part II

Implementations: Unitary Control

Chapter 4

Freezing a quantum magnet by repeated quantum interference

This chapter is about the work on experimental realization of a new quantum phenomenon known as dynamical many-body freezing using a 3-qubit NMR simulator [12].

4.1 Introduction

When a classical system is perturbed by an external periodic drive with frequencies much higher than the characteristic frequencies of the system, the system does not get sufficient time to adjust itself within the drive period. In other words, the system does not respond to the external drive and hence freezes for all such drive frequencies. However, a recent theoretical study showed that when a quantum many-body system, particularly a 1-dimensional spin chain, is driven by a periodic field with a frequency much higher than the characteristic frequencies of the system, the system exhibits a peculiar response behaviour as opposed to the calssical case [30]. Under the above mentioned case and for specific drive parameters, the systems freezes for all times and for arbitrary initial states due

System	Low ω regime	High ω regime
Classical	Responds	Freezes
Quantum	Responds	Freezes & Responds

Table 4.1: Difference between classical and quantum many-body response under the influence of external periodic field with ω being its frequency. The terms 'low' and 'high' are with respect to the characteristic frequencies of the system under consideration.

to the phenomenon of dynamical many-body freezing (DMF) [12]. Moreover, unlike classical case, it was also shown that the quantum many-body systems responded as well as froze even in the above mentioned scenario. The comparison between the clasical and quantum case is briefly summarized in table 4.1 and the same comparison in the specific case of fast external drives is shown in the Fig. 4.1. As was previously studied, this non-monotonicity in the response of the quantum many-body systems under the an external periodic drive is attributed to the phenomenon of quantum interference [30]. In this chapter, I will explain the experimental demonstration of this phenomenon that was carried out in our lab [12].

Freezing of the particle under the action of external periodic drive was previously observed. Examples include dynamical localization of a single particle [35] and coherent destruction of tunneling of a single particle [36]. However the phenomenon of dynamical many-body freezing differs from the above as follows: It is a quantum many-body problem. The freezing occurs for all times and for arbitrary initial states for specific drive parameters.

The motivation to demonstrate this phenomenon is two fold:

- The field of driven quantum many-body systems is still largely unexplored. Despite the experimental challenges, we successfully simulated this phenomenon using a 3-qubit NMR simulator for the first time.
- The experimental feasibility of controlling the quantum systems by tuning the drive parameters opens up the possibilities of a novel quantum control

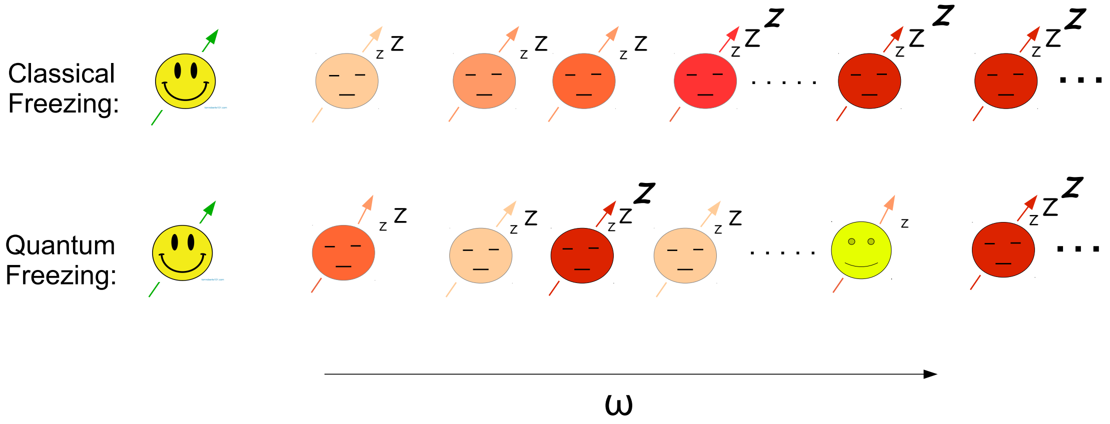

Figure 4.1: Classical (top row) and quantum (bottom row) systems under the influence of fast drives corresponding to high ω regime. Each smiley represents a many-body system. The horizontal axis corresponds to the drive frequency (ω). The superscripts in the smilies refer to the response: while three 'z's in the superscripts represent fully frozen systems, the absence of superscript represent a responding system and the two 'z's correspond to intermidiate cases. The classical systems freezes for all high frequencies but in the quantum case, the systems freeze and respond non-monotically.

techniques.

Below, I shall explain the basic theoretical outline of the phenomenon of DMF through numerical simulations. I will also numerically show how the main quantity of interest deviates in the presence of experimental errors and how it can be overcome.

4.2 Numerical simulations

4.2.1 Quantifying freezing

This section gives the necessary details required to quantify the amount of freezing. We consider a quantum many-body system in one dimension that is evolving under a specific Hamiltoninan starting from an arbitrary initial state. By monitoring the magnetization corresponding to the instantaneous states at regular intervals, we quantify the amount of freezing for specific Hamiltonian parameters by calculating the long time average of the magnetization, called as dynamical order parameter Q [30]. We see that the non-monotonic response of the driven quantum many-body system by a periodic field in captured by Q.

Consider an infinite one dimensional Ising spin chain subjected to a transverse periodic field. Such a system is described by the Hamiltonian

$$\mathcal{H}(t) = -\frac{1}{2}[\mathcal{J}\sum_{i}^{n-1}\sigma_i^z\sigma_{i+1}^z + h_0\cos(\omega t)\sum_{i}^{n}\sigma_i^x], \tag{4.1}$$

where $n = \infty$ is the number of spins, $\mathcal{J}$ is the coupling between the nearest neighbouring spins, h_0 is the drive amplitude and ω is the drive frequency.

Starting from an initial state $\rho(0)$, the infinite one dimensional spin chain evolves under the action of the Hamiltonian $\mathcal{H}(t)$. The final state is $\rho(t)$ and we study the response of the system in terms of its transverse magnetization $m^x(t)$. As previously mentioned, the quantity that characterizes the strength of freezing is Q which is defined as a long time average of $m^x(t)$ and is given by

$$Q = \lim_{\mathcal{T}\to\infty}\frac{1}{\mathcal{T}}\int_0^{\mathcal{T}} m^x(t)dt, \tag{4.2}$$

where $\mathcal{T}$ is the total evolution time.

The freezing case requires that $m^x(t)$ remains the same as $m^x(0)$ for all times t. Thus it implies that $Q = 1$ for the freezing case. However, when $m^x(t)$ oscillates, $Q < 1$ and thus corresponds to the non-freezing case.

A closed form for Q was analytically derived by A. Das [30] for an infinite spin Ising chain and is given by

$$Q_\infty = \frac{1}{1 + |J_0(2h_0/\omega)|}, \tag{4.3}$$

where J_0 is the zeroth order Bessel's function. Thus the non-monotonic feature of J_0 imposes non-monotonicity in Q.

Fig. 4.2 shows the numerical plot for Q vs ω. The solid line corresponds to the $n = \infty$ case. This plot considers the high frequency regime where ω values are much higher than the maximum characteristic frequency of the system given by $2\mathcal{J}$.

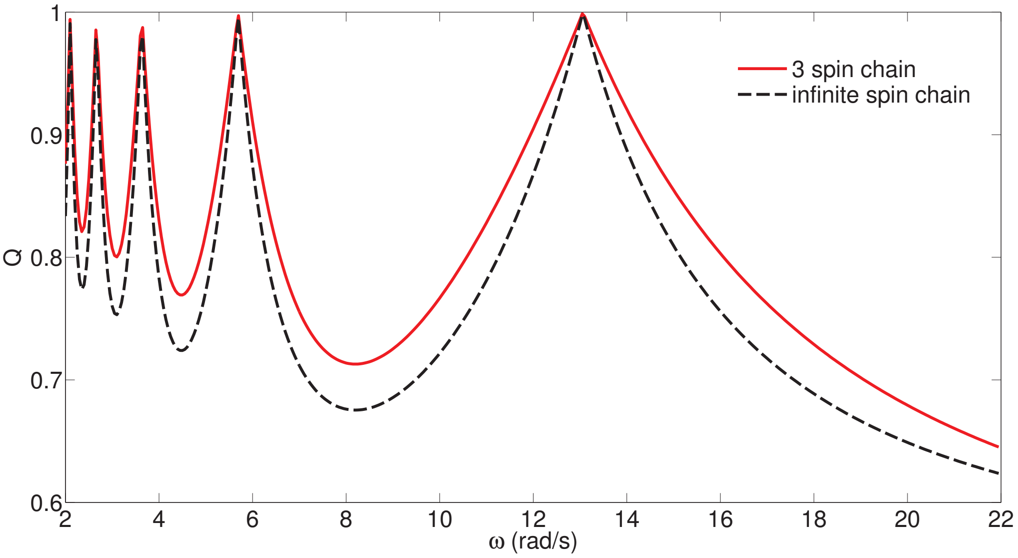

Figure 4.2: The non-monotonic behaviour of Q with ω for finite and infinite spin chain in the high frequency regime. The simulation is done for the parameters corresponding to $h_0 = 5\pi$ and $\mathcal{J} = h_0/20$, both in units of rad/s, that are consistent with strong ($h_0 \gg \mathcal{J}$) and fast ($\omega \gg 2\mathcal{J}$) drive scenario.

Similarly, the analytical form for Q for a finite spin chain ($n = 3$) was shown to be

$$Q_3 = \frac{1 + |J_0(2h_0/\omega)|}{1 + 3|J_0(2h_0/\omega)|}. \tag{4.4}$$

As seen from Fig. 4.2, the Q vs ω plot for $n = 3$ is similar to that of the infinite spin chain. This feature of Q being independent of n as is refelcted in Eq. 4.3 and 4.4 allowed us to study this phenomenon on a small scale 3-qubit NMR quantum simulator.

4.2.2 Experimental challenges

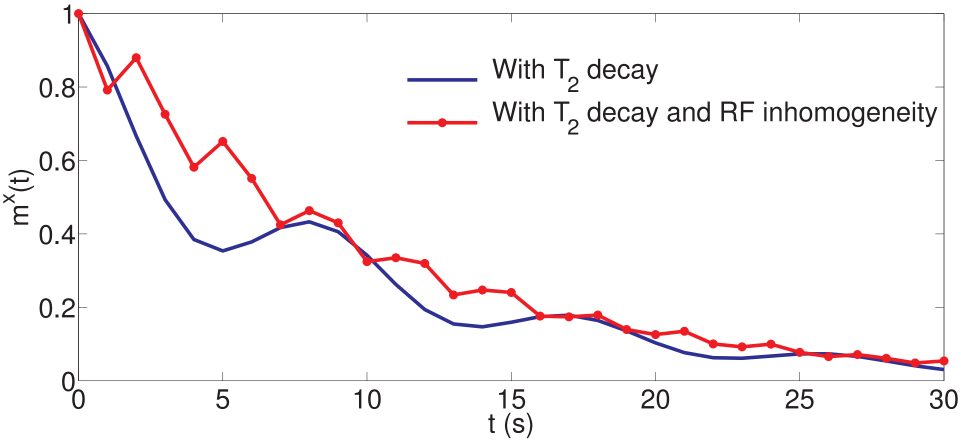

Figure 4.3: Numerical simulation of the evolution of magnetization for $\omega = 8.4$ and in the presence of errors for $h_0 = 5\pi$ and $\mathcal{J} = h_0/20$ starting from an initial state $\rho(0) = \sum_i^3 \sigma_i^x/2$.

The heart of quantum simulation protocol lies in the efficient implementation of the dynamics corresponding to a specific Hamiltonian. Here, the Hamiltonian of interest is given by Eq. 4.1 and the corresponding unitary operator is $U(t) = \mathcal{T} e^{-i\int_0^t \mathcal{H}(t')dt'}$ where $\mathcal{T}$ is the time ordering operator. In NMR setup, this $U(t)$ is realized by RF pulses which are specified by definite amplitudes and phases. However, in practice, realizing $U(t)$ with a specific implementation time t is a challenging problem due to inherent decoherence and due to external imperfect pulses. While imperfect pulses are due to RF inhomogeinity, the decay in magnetization is due to the decoherence.

Fig. 4.3 shows the numerical simulation of $m^x(t)$ in the presence of errors. By incorporating 20% RF inhomogeneity and a decay constant with $T_2 = 10s$, we see that the non-freezing point corresponding to $\omega = 8.4$ rad/s is adversely affected by the errors with no sign of oscillations in $m^x(t)$. Similarly, Fig. 4.4 shows how the effect of RF inhomogeneity changes the freezing points. While the plots with only T_2 decay still captures the response correctly, the plots with

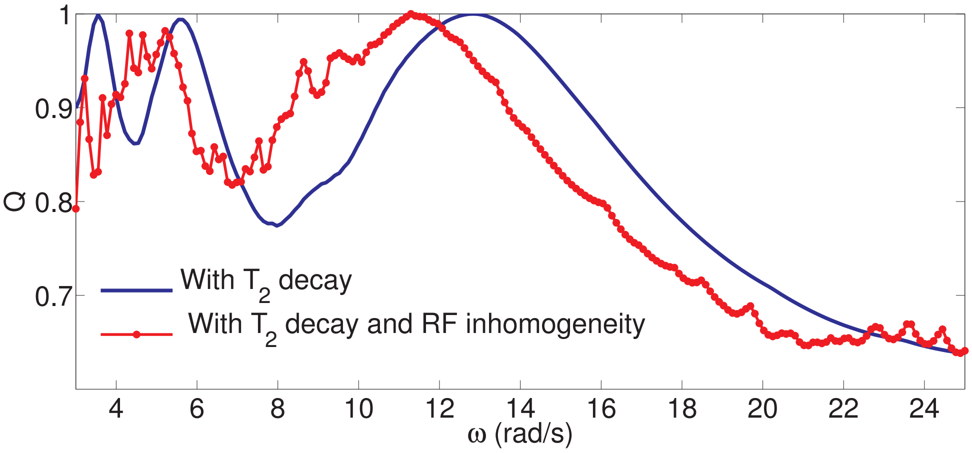

Figure 4.4: Numerical simulation for Q vs ω by incorporating errors for $h_0 = 5\pi$ and $\mathcal{J} = h_0/20$ starting from an initial state $\rho(0) = \sum_i^3 \sigma_i^x/2$.

T_2 decay and RF inhomogeneity show an erratic response. This indicates that the pulses imperfections produce worse effects as compared to the decoherence effects.

Thus experimental implementaion of this phenomenon demands for an efficient control technique that are robust against RF inhomogeneities.

4.2.2.1 Overcoming the challenge

In order to circumvent the above problem, we used an optimal control algorithm called GRadient Ascent Pulse Engineering (GRAPE). This algorithm generates high fidelity, robust amplitudes and phase modulated RF pulses.

Consider an $n-$ qubit NMR system defined by the Hamiltonian:

$$H = H_0 + \sum_{k=1}^{m} u_k(t) H_k, \tag{4.5}$$

where H_0 is the internal Hamiltonian and H_k is the control Hamiltonian corresponding to the

4.3 Quantum simulation

The simulation protocol for a 3-qubit simulator involves the following main steps:

1. Initial state preparation:

   We performed two sets of experiments with different initial states $\rho(0)$, i.e., for $\rho(0) = \sum_i^3 \sigma_i^x/2$ and for $\rho(0) = \sum_i^3[\sigma_i^x/2 + \sigma_i^z\sqrt{3}/2]$. These correspond to the initial transverse magnetization values $m^x(0) = 1$ and $m^x(0) = 0.5$ respectively. Note: General form of $m^x(t)$ is given by $m^x(t) = \mathrm{Tr}[\rho(t)(\sum_i^3 \sigma_i^x/2)]$.

2. Unitary implementation:

   The unitary $U(t)$ corresponding to $\mathcal{H}(t)$ given by Eq. 4.1 is $U(t) = \mathcal{T}e^{-i\int_0^t \mathcal{H}(t')dt'}$ where $\mathcal{T}$ is the time ordering operator. In order to be consistent with the fast drive, we specifically chose the Hamiltonian parameters as follows: $h_0 = 5\pi$, $\mathcal{J} = h_0/20$. Note that $\omega \gg 2\mathcal{J}$, the maximum characteristic frequency of the system under consideration.

   The idea is to simulate the solid curve in Fig. 4.2 experimentally. Suppose we consider a particular value of ω and observe the 3-qubit system. We implemented this dynamics by generating the corresponding $U(\tau)$ for a time $\tau = 2\pi/\omega$. Since the terms in $\mathcal{H}(t)$ do not commute with each other, the imlpementation of $U(t)$ requires descritization of t into smaller time intervals. We discretized τ into 11 equal intervals and thus $U(\tau) = U_{11}\cdots U_2U_1$ where each $U_j = e^{-i\mathcal{H}(m)m}$ with $m = \tau/11$. Thus the dynamics was realized by implementing $U(\tau)$ j times with $j = 0, 1, \cdots, N$ where $N = 30$ for a total time of $T = j\tau$. Thus $\rho(0)$ evolves under $U(j\tau)$ as

   $$\rho(j\tau) = U(j\tau)\rho(0)U(j\tau)^\dagger = U(\tau)^j\rho(0)[U(\tau)^\dagger]^j \tag{4.6}$$

3. Read-out:

We measured $m^x(j\tau)$ at regular intervals $t = j\tau$ with $j = 0, 1, \cdots, N$ which is given by

$$m^x(j\tau) = \mathrm{Tr}[\rho(j\tau)\sum_i^3 \sigma_i^x/2], \tag{4.7}$$

and hence Q becomes

$$Q = \frac{1}{N+1}\sum_{j=0}^{N} m^x(j\tau). \tag{4.8}$$

Below, I will explain how this protocol was used to simulate this dynamics using a 3-qubit NMR simulator in liquid state.

4.4 Experiments and Results

Our quantum simulator consisted of three ^{19}F nuclear spins in the molecule tifluoroiodoethylene and its properties are shown in Fig. 4.5. The molecule is dissolved in acetone-D6 and all the experiments were carried out in Bruker 500 MHz NMR spectrometer at an ambient temperature of 290 K.

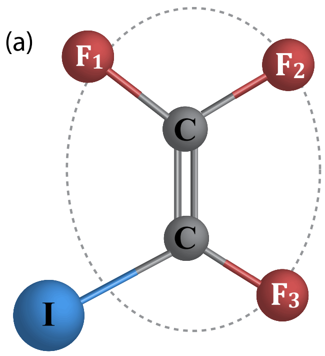

Figure 4.5: Molecular structure of tifluoroiodoethylene.

The internal Hamiltonian for this NMR system is given by

$$H_0 = -\pi \sum_{i=1}^{3} \nu_i \sigma_i^z + \frac{\pi}{2} \sum_{\substack{i,j=1 \\ i<j}}^{3} J_{ij} \sigma_i^z \sigma_j^z, \tag{4.9}$$

where the first term is the Zeeman Hamiltonian and the second term is the spin-spin interaction Hamiltonian.

We see that H_0 in Eq. 4.9 is different from $\mathcal{H}(t)$ in Eq. 4.1. Thus the simulation problem boils down to the realization of $\mathcal{H}(t)$ using H_0 and external RF controls. The first step is to cancel the evolution of the Zeeman Hamiltonian in Eq. 4.9.

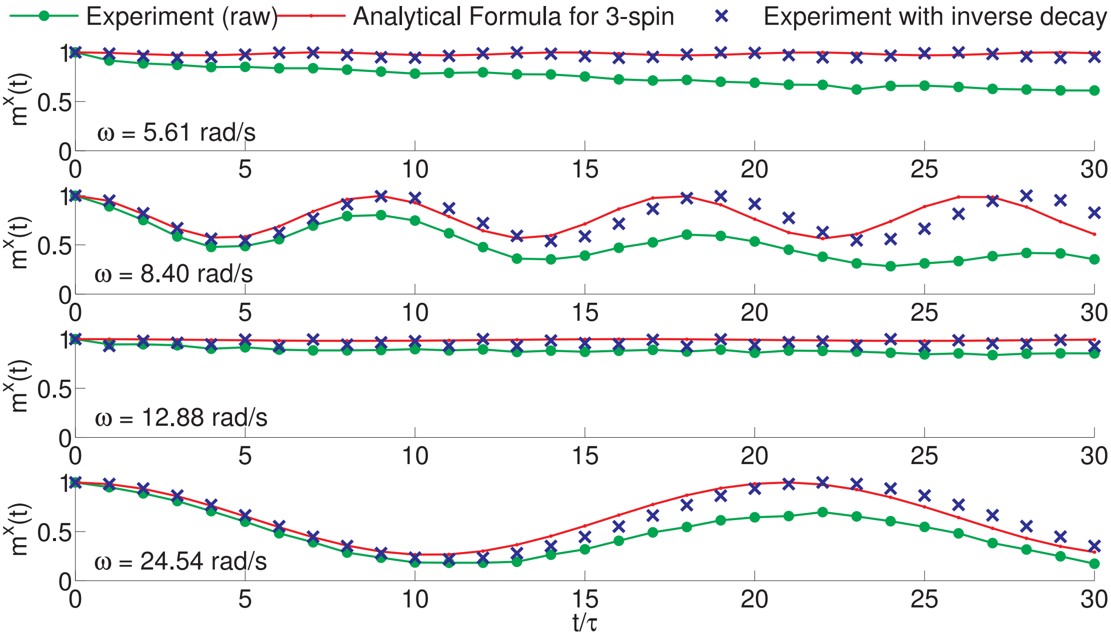

Figure 4.6

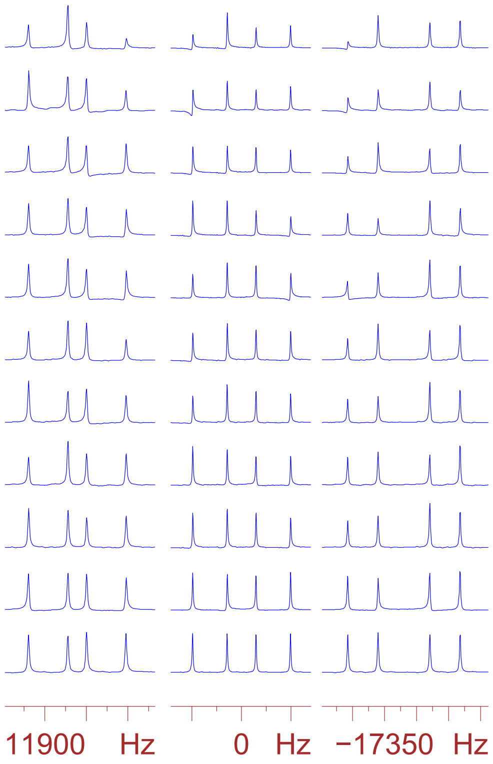

Figure 4.7

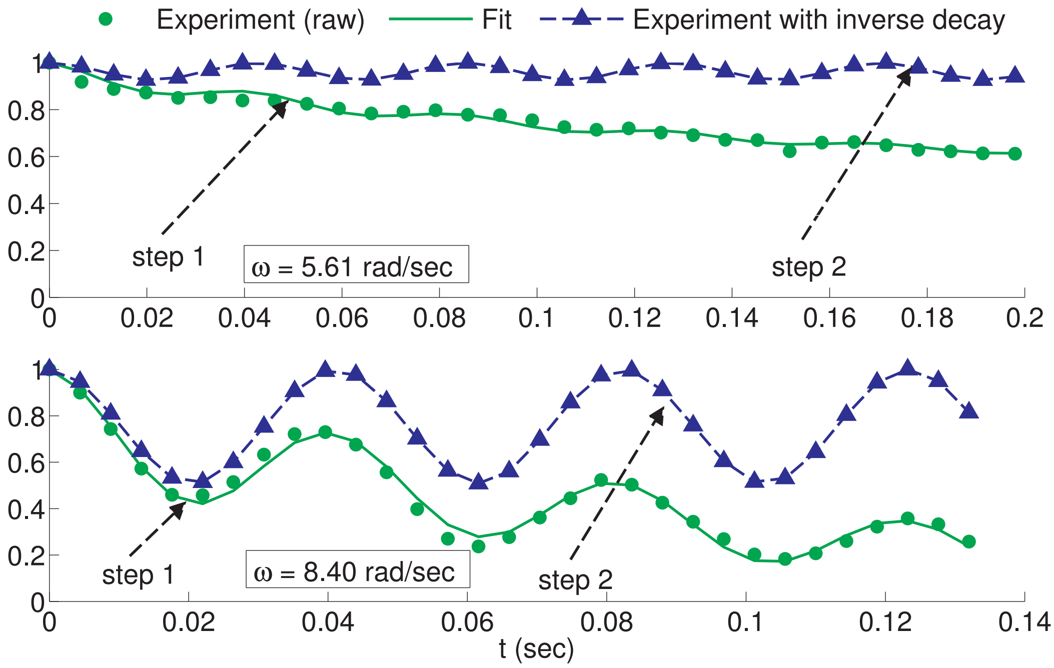
Experiment (raw)
Fit
Experiment with inverse decay
1
0.8
0.6
0.4
0.2
0
0.02
0.04
0.06
0.08
0.1
0.12
0.14
0.16
0.18
0.2
step 1
step 2
ω = 5.61 rad/sec
ω = 8.40 rad/sec
t (sec)

Figure 4.8

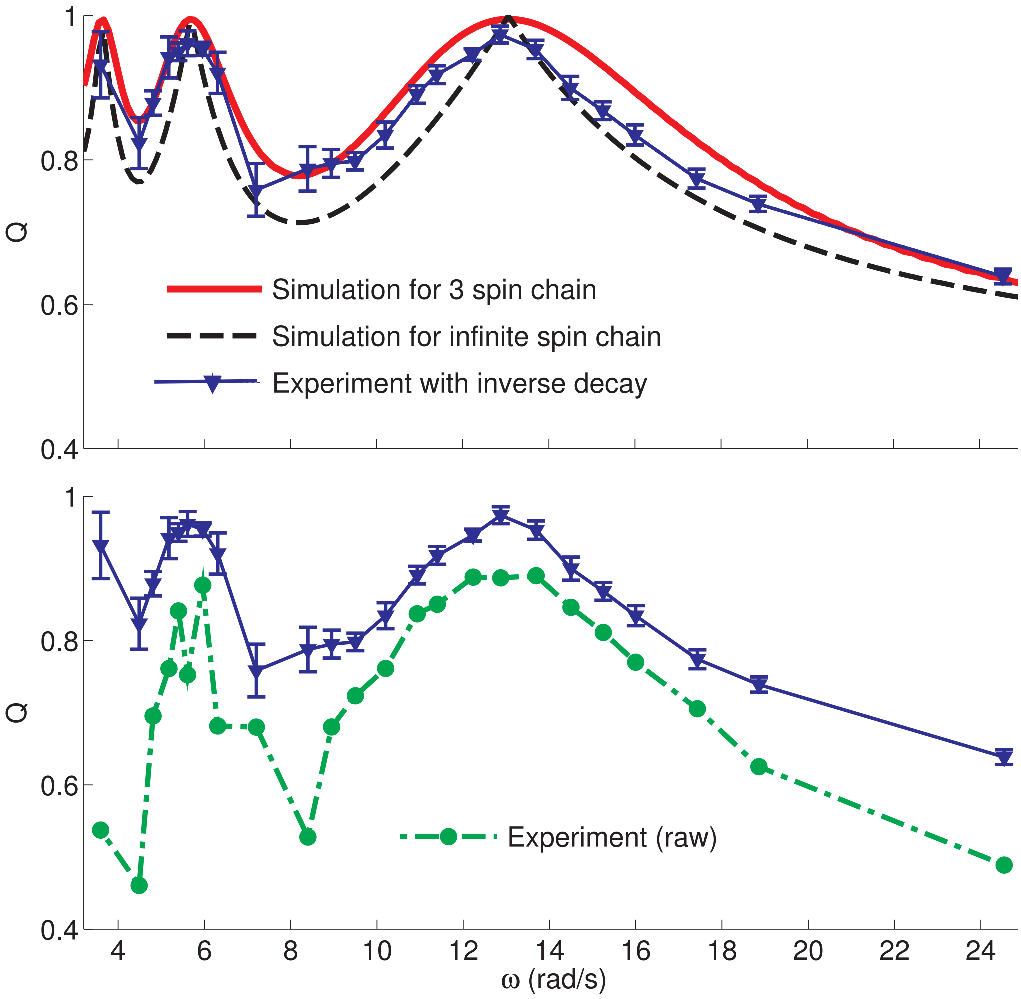
1
0.8
0.6
0.4
Q
Simulation for 3 spin chain
Simulation for infinite spin chain
Experiment with inverse decay
1
0.8
0.6
0.4
Q
Experiment (raw)
4
6
8
10
12
14
16
18
20
22
24
ω (rad/s)

Figure 4.9

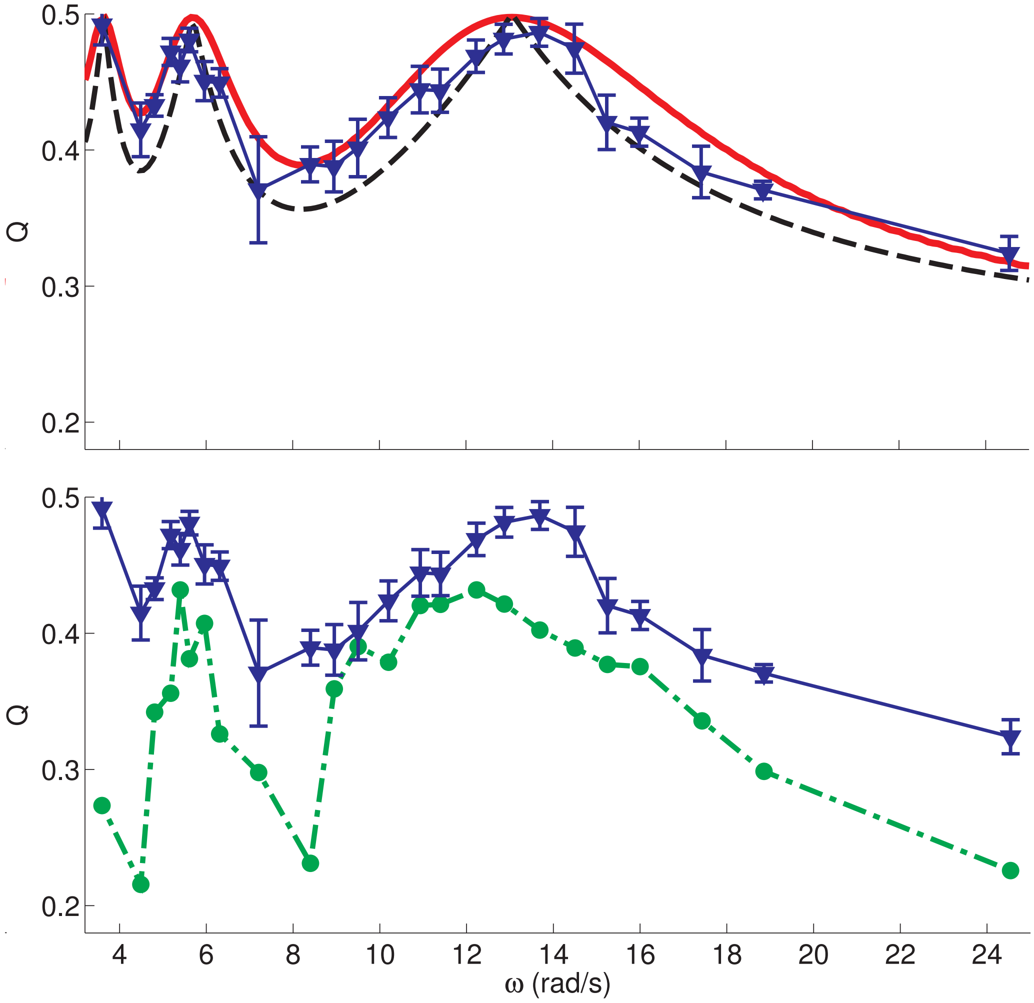

Figure 4.10

Chapter 5

Pauli Decomposition over Commuting Subsets: Applications in Gate Synthesis, State Preparation, and Quantum Simulations

5.1 Introduction

5.2 Motivation

5.3 Theoretical outline and numerical simulations

5.4 Experiments and Results

5.5 Conclusions

Part III

Implementations: Non-unitary Control

Chapter 6

Engineered decoherence: Characterization and suppression

6.1 Introduction

Quantum devices which are perfectly isolated from their environment follow unitary dynamics wherein the probabilities and coherences of the density operators are preserved throughout the state evolution. This is the ideal case that is strongly desired in the field of quantum computation and communication. However, in practice, no quantum device is perfectly isolated from its environment. This leads to inevitable interactions between a quantum system and the environment which ultimately entangles the two. For sufficiently large times and for large environmental size, the evolution of quantum system becomes non-unitary leading to an irreversible information transfer from the quantum system to the environment.

The most common information losses correspond to the coherence decay, also known as phase decoherence, and energy dissipation of the quantum systems. The decay constants T_1 and T_2 are associated with energy dissipation and decoherence processes respectively, that are borrowed from NMR terminology (section. ref) [37]. In general, $T_1 > T_2$ which implies that the quantum systems lose phase information faster than their energy. Hence in any quantum information protocol it is important to implement the gates within the time scale of T_2. The very fact that the phenomenon of decoherence has been a severe threat to the physical realization of a quantum computer has lead towards several theoretical and experimental studies on decoherence [31, 38, 39, 40, 41, 42, 43].

In this chapter, I will explain our work that deals with the understanding of phase decoherence and is organized into three parts:

1. We experimentally simulated artificial phase decoherence. Although, in practice, one does not have any control over the environment, emulation of decoherence gives a direct control over it. By systematically controlling the environment one can study its effects on the system coherences.

2. we suppressed the induced decoherence using standard dynamical decoupling (DD) sequences. The simultaneous competition between the DD sequences and the decoherence process might give insight into the decoherence process and ways to improve DD sequences.

3. We characterized the amount of the induced decoherence in the system qubits using noise spectroscopy (NS) and quantum process tomography (QPT). NS gives the frequency distribution of the noise and QPT gives the entire information of the noise process for a specific noise frequency.

We implemented the above steps using a 2-qubit NMR simulator. The model considered one qubit as a system qubit and the other as an environment qubit. Additional decoherence, apart from the inherent decoherence, was induced using random classical fields on the enviromnet qubit [31]. We studied the effect of controlled noise on the system qubit. In the following sections, I will introduce to decoherence model, DD sequences, NS, QPT, and experiments, and results.

6.2 Decoherence models

In this section, I will explain the phase decoherence model with ZZ type system-environment interaction.

6.2.1 Zurek's decoherence model

This model was given by Zurek [44] and is explained below.

Consider an n qubit composite system consisting of two subsystems. One qubit is considered as the system of interest and the rest of the qubits are considered as the environment. The total Hamiltonian and the correspoding unitary operator is respectively given by

$$H_{SE} = \sum_{j=2}^{n} J_{1j} Z_1 Z_j \qquad \text{and} \qquad U_{SE}(t) = e^{-iH_{SE}t}. \tag{6.1}$$

Here J_{1j} is the coupling between the system (represented by subscript 1) and the environment (represented by subscript j). Zurek showed that the Hamiltonian with ZZ type system-environment interaction leads to phase decoherence.

Let the combined system start with a separable state:

$$|\psi(0)\rangle_{SE} = |\psi(0)\rangle_S \otimes |\psi(0)\rangle_E. \tag{6.2}$$

Here the pure state $|\psi(0)\rangle_S = a|0\rangle_1 + b|1\rangle_1$ with $|a|^2 + |b|^2 = 1$ is the system state and $|\psi(0)\rangle_E = \Pi_{j=2}^{n}(\alpha_j|0\rangle_j + \beta_j|1\rangle_j)$ with $|\alpha_j|^2 + |\beta_j|^2 = 1$ is the environment state.

The evolution of $|\psi(0)\rangle_{SE}$ under the U_{SE} entangles the system and the environment as below:

$$\begin{aligned}|\psi(t)\rangle_{SE} &= U_{SE}(t)|\psi(0)\rangle_{SE} \\ &= a|0\rangle_1\Pi_{j=2}^{n}(\alpha_j e^{-iJ_{1j}t}|0\rangle_j + \beta_j e^{iJ_{1j}t}|1\rangle_j) \\ &+ b|1\rangle_1\Pi_{j=2}^{n}(\alpha_j e^{iJ_{1j}t}|0\rangle_j + \beta_j e^{-iJ_{1j}t}|1\rangle_j) \end{aligned} \tag{6.3}$$

The corresponding density operator is given by $\rho_{SE}(t) = |\psi(t)\rangle_{SE}\langle\psi(t)|_{SE}$ and the system density operator $\rho_S(t)$ is obtained by tracing out the environment subsystem from $\rho_{SE}(t)$, i.e., $\rho_S(t) = \mathrm{Tr}_E[\rho_{SE}(t)]$. The quantity that we are interested in is the coherence part of the density operator. As was already mentioned in Eq. 2.7, the off-diagonal term ρ_S^{01} encodes the coherence information and this matrix element in Z basis is given by

$$\begin{aligned}\rho_S^{01}(t) &=_1 \langle 0|\rho_{SE}(t)|1\rangle_1 \\ &= ab\cdot\Pi_{j=2}^{n}(|\alpha_j|^2 e^{-2iJ_{1j}t} + |\beta_j|^2 e^{2iJ_{1j}t}) \\ &= ab\cdot z(t), \end{aligned} \tag{6.4}$$

where $\{|0\rangle_1, |1\rangle_1\}$ are the basis states of the system qubit and $z(t)$ is called as the decoherence factor. As seen from the above equation, $|z(t)| \to 0$ implies the decay in the coherences of the initial system state $|\psi(0)\rangle_S$ after time t. Further, it can also be noted that irreversible decoherence can occur when $n \to \infty$, i.e., when the environmental size is large.

6.2.2 Simulation of decoherence

As was already discussed, Zurek's decoherence model requires large environmental size for irreversible phase damping. However, an important question in experimental realization is whether one can still simulate the same process using only finite sized environment. In this section, I will give a brief review of the methods given by Teklemariam *et al.* [31] to emulate artificial decoherence even when the environment size is finite. Such finite sized decoherence simulation allows for the direct control over the environment that can be eaisily implemented in laboratory with a goal to study the deoherence process.

The model given by Teklemariam *et al.* differs from the Zurek's model as follows: Suppose, the dimension of the Hilbert space of the quantum system is 2^n. The model considers its interaction with environment described by a maximum Hilbert space dimension of 2^{2n}. This greatly restricts the size of the environment for very small n but favors experimental studies on decoherence. Further, in order to mimic infinite sized environment and to induce irreversible phase damping from the system qubits, this model uses additional stochiastic classical fields on the environment.

For the sake of simplicity, consider a two qubit system-environment model initially in the product state,

$$\rho_{SE}(0) = \rho_S(0) \otimes \rho_E(0), \tag{6.5}$$

Initailly the composite system is assumed to be a closed system and the total Hamiltonian is given by

$$\mathcal{H} = \pi(\nu_S Z_S + \nu_E Z_E + \frac{J}{2} Z_S Z_E), \tag{6.6}$$

where ν_S and ν_E are the resonant frequenceis of the system (S) and the environment (E) qubits respectively, and J is the strength of the coupling between the two. We consider the Hamiltonian in the rotating frames where $\nu_S = \nu_E = 0$. The state $\rho_{SE}(0)$ evolves under the propagator $U(T)$ for a total time T which is given by

$$U(T) = e^{-i\mathcal{H}T} \tag{6.7}$$

that entangles S and E as was discussed in section 6.2.1.

Suppose, E is perturbed by random classical fields without externaly disturbing S. These perturbations are called as kicks and each kick operator K_m corresponds to the rotation of E with an arbitrary rotation angle ϵ_m about y-axis. For the m^{th} kick, we have $K_m = \mathbb{I}_S \otimes e^{-i\epsilon_m Y_E}$ where $\mathbb{I}_S$ is the Identity on the system and ϵ_m is chosen randomly between $[-\alpha, \alpha]$ with α being a small angle.

The kicks are assumed to be instantaneous with the kick rate $\Gamma = k/T$ where k is the total number of kicks. Under this action, Eq. 6.7 is modified to incorporate its dependency on the random angles ϵ_m and is given by

$$U_k(T) = K_k U(\delta) K_{k-1} U(\delta) \cdots K_1 U(\delta); \qquad \delta = \frac{T}{k}. \tag{6.8}$$

A state $\rho_{SE}(0)$ evolves under this operator as $\rho_{SE}(T) = U_k(T)\rho_{SE}(0)U_k(T)^\dagger$ and the system and environment states are given by $\rho_S(T) = \mathrm{Tr}_E[\rho_{SE}(T)]$ and $\rho_E(T) = \mathrm{Tr}_S[\rho_{SE}(T)]$ respectively.

An ensemble realization over many random $\epsilon_m \in [-\alpha, \alpha]$ leads to an average behavior represented by

$$\bar{\rho}_s(T) = \int_{-\alpha}^{\alpha} \frac{d\epsilon_k}{2\alpha} \cdots \int_{-\alpha}^{\alpha} \frac{d\epsilon_1}{2\alpha} \mathrm{Tr}_E[U_k \rho_S(0) U_k^\dagger]. \tag{6.9}$$

Teklemariam *et al.* showed that [31],

$$\bar{\rho}_S(T) = \sum_{r,s=0,1} D_{rs}(k,T) \rho_S^{rs}(0) |r\rangle\langle s|, \tag{6.10}$$

with $|r\rangle$, $|s\rangle \in \{|0\rangle, |1\rangle\}$ being the eigenstates of Z_S and $D_{rs}(k,T)$ is the decoherence factor which is given by

$$D_{rs}(k,T) = \mathrm{Tr}_E[\mathcal{O}^k(\rho_E(0))]. \tag{6.11}$$

Here $\mathcal{O}$ is the superoperator that is neither trace preserving nor Hermitian and its action is defined as $\mathcal{O}(\rho_E) = cV_K\rho_E V_K + dYV_K\rho_E V_K Y$ with $V_K = e^{-i\pi J\delta Z_E/2}$,

$c + d = 1$, $c - d = \gamma$, and $\gamma = \sin(2\alpha)/(2\alpha)$. This indicates that for a specific value of ϵ, J and γ, one can simulate a unique type of phase decoherence.

Teklemariam *et al.* showed that for smaller ϵ's and for lower Γ, the decoherence rate $1/T_2$ was proportional to Γ. However, for certain Γ value, $1/T_2$ saturated and for a much higher Γ value, $1/T_2$ decreased exponentially with Γ. Thus the former case correspond to the decoherence inducing effect while the latter case corresponded to noise decoupling effect. This latter case was not explored in our work due to the experimental limitations considering the fact that very high kick rates could damage the RF-coils in NMR setup.

6.3 Suppressing Decoherence

Preserving the qubit information against noise is one of the important steps in quantum information processing. Different techniques have been developed to suppress decoherence like dynamical decoupling (DD) [45, 46], quantum error correction [47], use of robust approaches such as adiabatic quantum computation [48], or encoding quantum information in decoherence-free subspaces [49]. In this chapter, I will explain two standard DD techniques that are utilized in our work in order to suppress the inherent as well as induced artificial decoherence. One of the major advantages of this technique is that unlike the other techniques, DD does not require extra qubits and it can be combined with other quantum gates leading to fault tolerant quantum computation [50, 51].

I will first explain a way to suppress the static noise, a technique known as Hahn echo sequence. However, in practice, the noise is time-dependent. I will explain two standard DD techniqes for suppressing time-dependent noise, namely CPMG and Uhrig DD sequences. All these techniques are explained in the case of NMR setp-up.

6.3.1 Hahn Echo

A technique to suppress time-independent noise in a single qubit was given by Hahn [52]. Suppose the static magnetic field B_0 has a spatial inhomogeneity (NMR set-up). This small change in B_0 changes the larmor frequencies of the nuclei and hence different nuclei experience different larmor frequencies (section ref). However the desired scenario is the case wherein all the nuclei coherently behave as one single nuclei and precess with the same larmor frequency. In order to achieve this, Hahn gave a sequence as shown in Fig. 6.1.

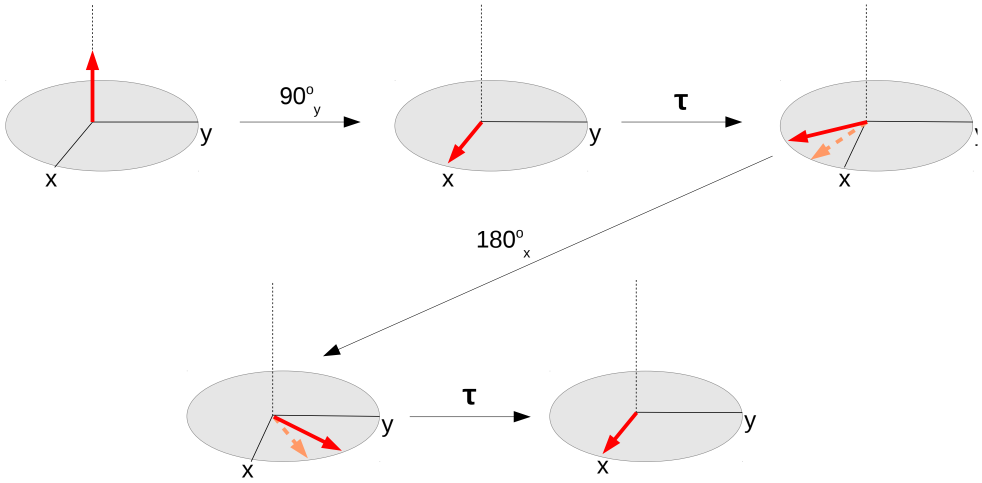

Figure 6.1: Evolution of the net magnetization (indicated by arrows) under the Hahn echo sequence. The dotted arow represents slow precessing spins and the solid arrow represents fast preseccing spins. In this case, the precession of the nuclei about the z-axis is assumed to be clockwise.

As shown in Fig. 6.1, the arrow represents the net magnetization of the single qubit nuclei in the NMR system and is initially oriented about the z-axis. The effect of the pulse sequence is explained as follows: The initial $\pi/2$ pulse about the y-axis rotates the nuclei to x-axis. This is follwed by free evolution of the spins for a time τ during which different nuclei will pick up different larmor frequencies in the presence of B_0 inhomogeneity. The nuclei fan-out with a range of larmor frequencies. The slow moving components are represented by dotted arrow and the fast moving are components represented by solid arrow. A π pulse about the x-axis rotates the spins and during the free evolution for time τ, the faster moving components catch-up with the slower moving components. Finally, all the spins are along the x-axis.

6.3.2 CPMG DD sequence

The term CPMG refers to Car-Purcell-Meiboom-Gill, named after the people who came up with a decoherence suppression technique when the noise is time-dependent [45]. This method is similar to Hahn echo except that CPMG DD consists of a train of equidistant π pulses that are applied on the system qubit as shown in Fig. 6.2. The π pulses are applied at regular intervals τ.

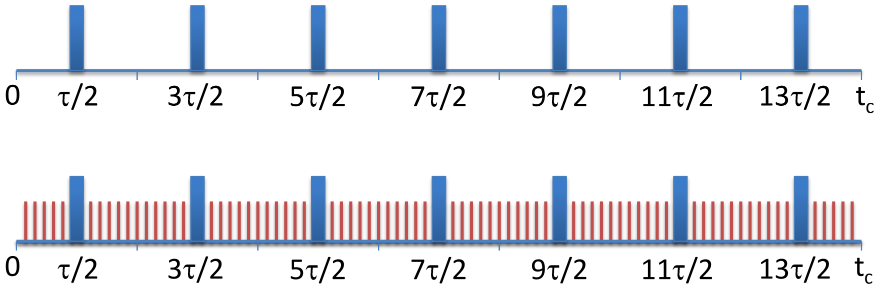

Figure 6.2: The top and bottom figures correspond to the CPMG DD pulse sequence in the absence and presence of kicks respectively for a cycle time of t_c and for $N = 7$. The solid bars indicate the π pulses that are applied on the system qubit and the vertical lines indicate the kicks on the enviroment qubit.

A CPMG sequences with a τ value much shorter than the noise correlation time can suppress the corresponding noise. In general, the smaller the value τ, the larger the bandwidth of noise that is suppressed, and thus increases the efficiency of DD.

It is important to note that the phases of π pulses are chosen such that the initial state is stationary under the pulses, so that the DD sequence is robust against pulse errors. In other words, if the magnetization just before the CPMG sequence is about x-axis then the π pulses in Fig. **??** are appied about the x-axis and vice versa.

6.3.3 Uhrig DD sequence

Uhrigh DD (UDD) is another technique to suppress low-frequency noise [46]. Unlike CPMG DD, here the π pulses are not equidistant but the π pulse spacing is given by

$$t_j = t_c \sin^2\left[\frac{\pi j}{2(N+1)}\right], \tag{6.12}$$

where N is the total number of π pulses and t_c is the cycle time and Fig. 6.3 shows the pulse sequence for $N = 7$.

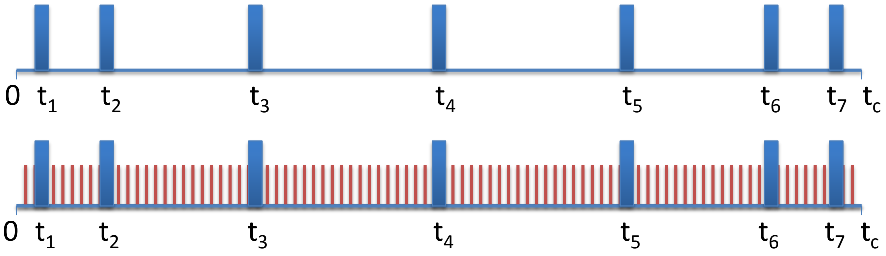

Figure 6.3: The top and bottom figures correspond to the UDD pulse sequence in the absence and presence of kicks respectively for a cycle time of t_c and for $N = 7$. The solid bars indicate the π pulses that are applied on the system qubit at instants t_i with $i = 1, 2, \cdots, N$ and the vertical lines indicate the kicks on the enviroment qubit. In both the cases only the T_2 of the system is measured. While the top figure is used to suppress the inherent decay, the bottom figure is used to suppress the inherent decay and the induced decay.

6.4 Characterizing decoherence

In this section, I will show how decoherence can be characterized using two techniques, i.e. by NS and QPT. NS gives the noise information in the qubit for different noise frequencies. Recently, NS has emerged to be of particular interest in quantum information processing due to its use in optimizing the DD sequences [53, 54, 55]. QPT gives the entire process. In our work, the process is decoherence process at particular noise frequency. This technique also quantifies the type of induced noise, e.g. bit flip or phase flip.

6.4.1 Noise spectroscopy

NS gives the frequency distribution of the noise which essentially contains the information about qubit noise content. Yuge *et al.* [33] and Alvarez *et al.* [32] independently proposed the method to experimentally measure the noise spectrum. Noise spectrum is defined by the quantity $S(\omega)$ which is a function of noise frequency ω. Higher the value of $S(\omega)$, higher is the noise content in the system of interest.

We utilize the method given by Yuge *et al.*. Fig. 6.8 shows the pulse sequence to measure $S(\omega)$. This sequence is basically CPMG sequence and is used to measure the decay constant T_2. As already mentioned in section 6.3.2, CPMG sequence increases T_2 by suppresses the noise and this depends on the value of τ where τ is the time interval between the consecutive π pulses. Thus by varying τ, one can have a distribution of T_2 values. Further, it was shown that [33]

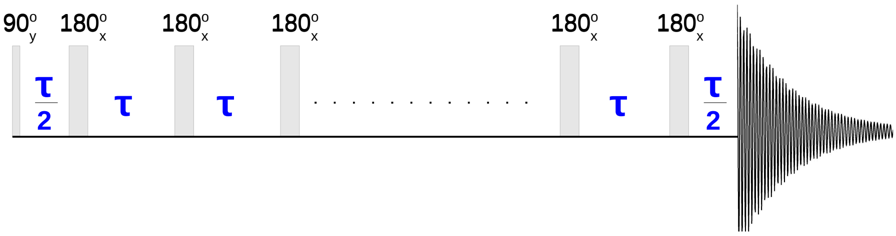

Figure 6.4: Pulse sequence to measure $S(\omega)$.

$$S(\omega) = \frac{\pi^2}{4T_2(\omega)}, \tag{6.13}$$

where $\omega = \pi/\tau$. Thus by scanning a range of ω and by measuring $T_2(\omega)$, one can obtain $S(\omega)$.

6.4.2 Quantum process tomography

QPT is a technique to reconstruct the entire quantum process [6].

Consider a quantum operation $\mathcal{E}$ which transforms the initial state ρ to a final state ρ' as follows:

$$\rho' = \mathcal{E}(\rho). \tag{6.14}$$

$\mathcal{E}$ can be any process which can either be unitary or non-unitary. The goal of quantum process tomography is to determine $\mathcal{E}$ [6, 56].

Suppose,

$$\mathcal{E}(\rho) = \sum_j E_j \rho E_j^\dagger; \qquad \text{where} \quad E_j = \sum_m e_{jm} \tilde{E}_m. \tag{6.15}$$

Here $\tilde{E_m}$ are the fixed set of operators and e_{jm} are the complex numbers. Hence

$$\mathcal{E}(\rho) = \sum_{mn} \tilde{E_m} \rho \tilde{E_n}^\dagger \chi_{mn}; \qquad \chi_{mn} = \sum_j e_{jm} e_{jn}^*. \tag{6.16}$$

Thus one can see that for a fixed set of operators $\tilde{E_j}$, one needs to determine the coefficients of χ. This is known as χ matrix representation.

After some algebra, one can deduce that

$$\sum_{mn} \beta_{pq}^{mn} \chi_{mn} = \lambda_{pq} \tag{6.17}$$

where,

- $\lambda_{pq} = \mathrm{Tr}[\rho_p^{'} \rho_q]$.
- $\beta_{rs}^{mn} = \mathrm{Tr}[\tilde{E}_m \rho_r \tilde{E}_n \rho_s]$.

In order to calculate λ_{pq}, one needs to know the final state ρ'. This characterization of ρ' is done by using quantum state tomography (QST) [6, 57, 58]. Since a single unknown quantum state cannot be characterized, QST involves the preparation of a large number of copies of ρ. For the sake of simplicity, I will briefly explain this procedure for a single qubit case.

As already mentioned in equation 2.5, a single qubit density operator has the form

$$\rho = \frac{1}{2}(\mathbb{I} + \sum_i r_i \sigma_i); \qquad \text{where} \quad r_i = \langle \sigma_i \rangle = \mathrm{Tr}[\rho\sigma_i].$$

Here, $\sigma_i \in \{X, Y, Z\}$. For the spin operators $\mathbb{I}/\sqrt{2}$, $X/\sqrt{2}$, $Y/\sqrt{2}$ and $Z/\sqrt{2}$, it follows that

$$\rho = \frac{\mathrm{Tr}[\rho]\mathbb{I} + \mathrm{Tr}[X\rho]X + \mathrm{Tr}[Y\rho]Y + \mathrm{Tr}[Z\rho]X}{2} \tag{6.18}$$

Thus characterizing ρ involves the measurements of the average value of the operator corresponding to $\mathbb{I}$, X, Y and Z which are given by $\mathrm{Tr}[\rho]$, $\mathrm{Tr}[X\rho]$, $\mathrm{Tr}[Y\rho]$ and $\mathrm{Tr}[Z\rho]$ respectively.

Thus, by solving β and λ, one can obtain the χ matrix. For an n- qubit system, χ will have $2^{4n} - 2^{2n}$ independent real parameters.

6.5 Experiments and results

The experiments were carried out on ^{13}C^{1}HCl$_3$ molecule dissolved in CDCl$_3$ at an ambient temperature of 300 K. The nuclei ^{13}C and ^{1}H form the two qubit system. The molecule and its properties are shown in Fig. 6.5.

We chose ^{1}H as our system qubit and ^{13}C as our environment qubit. Here, I will explain the three parts of our experimental work, i.e., introducing artificial phase decoherence in ^{1}H by randomly perturbing ^{13}C, Suppressing the decoherence in ^{1}H and finally characterizing the decoherence process that is induced in ^{1}H.

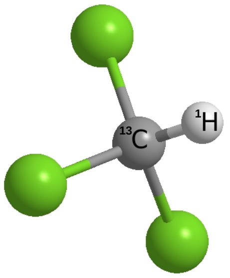

Figure 6.5: ^{13}C^{1}HCl$_3$ as NMR quantum simulator. The chemical shifts of ^{1}H and ^{13}C are 104.7 Hz and 0 Hz respectively. The J-coupling between the two is 209.4 Hz. The T_1 for ^{1}H and ^{13}C is 4.1s and 5.5s respectively, and T_2 for the same is 2.9s and 0.8s respectively.

The NMR Hamiltonian is similar to Eq. 6.19 and is given by

$$\mathcal{H} = \pi(\nu_H Z_H + \nu_C Z_C + \frac{J}{2} Z_H Z_C), \tag{6.19}$$

where ν_H and ν_C are the chemical shifts of the system (^{1}H) and the environment (^{13}C) qubits respectively, and J is the sclar coupling.

We prepared ^{1}H qubit in the initial state $\rho_H(0) = \mathbb{I}_H/2 + p_H X_H$ by applying a $\pi/2$ pulse about the y-axis on the thermal equilibrium state $\mathbb{I}_H/2 + p_H Z_H$. Here $p_H \sim 10^{-5}$ is the spin polarization. Also ^{13}C qubit was prepared in the initial thermal equilibrium state $\rho_C(0) = \mathbb{I}_C/2 + p_C Z_C$ where $p_C \sim 10^{-5}$.

Evolution under the action of kicks as explained in section 6.2.2 was realized by perturbing the ^{13}C qubit. These kicks were RF-pulses with random rotation angles and random phases. The experimental realization of artificial decoherence as explained in [31] is shown in Fig. 6.6.

We performed different sets of experiments with kicks corresponding to $\epsilon_m \in [0, 1^\circ], [0, 2^\circ]$ and random phases between 0 and 2π, while allowing the ^1H qubit to evolve freely.

Decoherence is observed by measuring its transverse magnetization $M_x(mt_c) = \mathrm{Tr}[\rho_H(mt_c) X_H]$ after m cycles each of duration t_c with $m = 0, 1, \cdots, N$ where

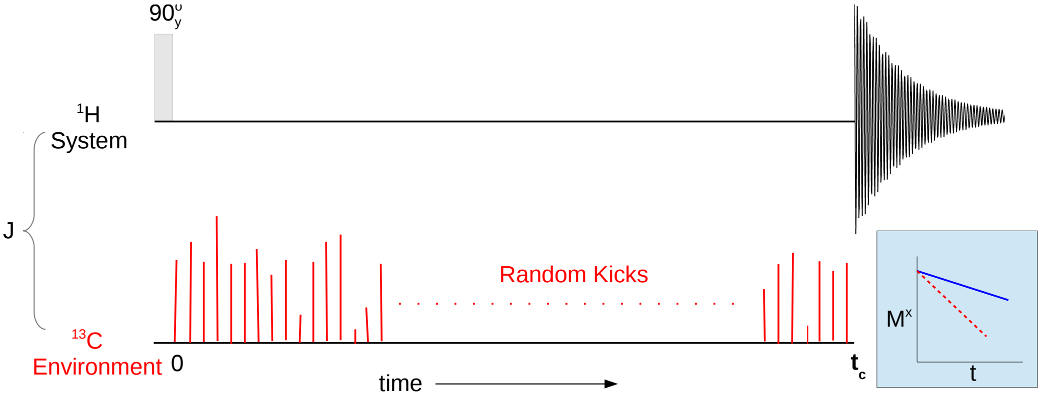

Figure 6.6: Method to introduce artificial decoherence. The filled bar on the system qubit corresponds to the RF pulse with rotation angle $90°$ about y-axis. This pulse prepares the system qubit in the required initial state. The vertical lines on the environment qubit are the random kicks applied for time t_c. The inset in the lower right corner represents the expected magnetization decay wherein the solid line corresponds to inherent decay and the dotted line corresponds to the inherent decay as well as decay due to the artificial decoherence.

N is total number of cycles. Fig. 6.7 shows the results of the experiment for $\epsilon \in [0°, 1°]$ and $\Gamma = 25$ kicks/ms (indicated by stars). As can be seen from the figure, the decay of magnetization is higher than that without kicks (indicated by filled circles) indicating that we introduced additional decoherence apart from the natural relaxation processes.

After emulating decoherence in ^{1}H, we suppressed it by using CPMG DD and UDD sequences. Figs. 6.2 and 6.3 shows the pulses sequences for implementing CPMG and Uhrig DD in the presence of kicks. While the π pulses were applied on ^{1}H, the kicks were applied on ^{13}C simultaneously. The experimental results as shown in Fig. 6.7 (indicated by open circles and boxes) show that the DD sequences were successful in suppressing decoherence even in the presence of kicks. Here, the efficiency of CPMG and UDD sequences are almost identical. It may be noted that detailed comparative studies of CPMG and UDD under natural relaxation processes have been studied elsewhere [59, 60]

As the last step, we characterized decoherence using NS and QPT. The way

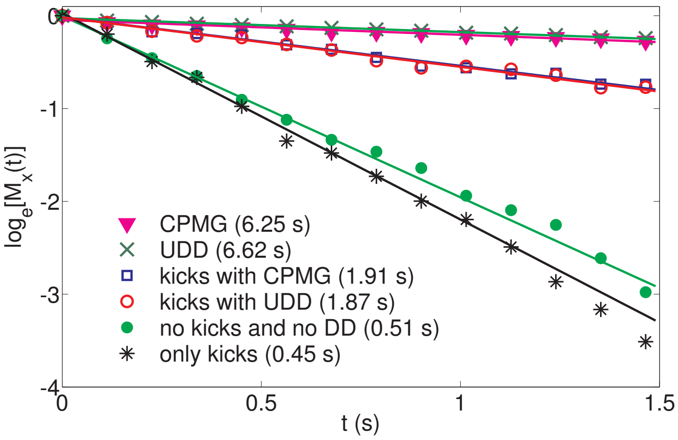

Figure 6.7: Decay of $M_x(t)$ under various cases. The numbers in the legend represent the T_2 values for the corresponding cases. The kick parameters are $\epsilon = [0°, 1°]$, $\Gamma = 25$ kicks/ms, and $t_c = 22.4$ ms and $\tau = 3.2$ ms.

to measure $S(\omega)$ as given in section 6.4.1 but in the presence of kicks on ^{13}C as shown in Fig. 6.8. T_2 of ^{1}H for each τ is obtained by fitting the experimental magnetization values to the decay model given by $M_x(t) = M_x(0)e^{-t/T_2}$, where $M_x(0)$ is the initial transverse magnetization. By vayring τ, we measured $T_2(\omega)$ where $\omega = \pi/\tau$ for various kick parameters.

Fig. 6.9 shows the noise spectral density distribution for various kick parameters. For comparison, we have also measured $S(\omega)$ in the absence of kicks (indicated by filled triangles). As expected, the $S(\omega)$ plot in the presence of kicks has higher values than that due to the inherent decay indicating that the effect of kicks is to induce noise. Generally, the noise spectra for the inherent noise has a Gaussian profile [61] and the results agree in the case of $S(\omega)$ of inherent decay. However, an interesting characteristic features in the noise spectral density at higher kick-rate (50 kicks/ms) were observed. Similar features were earlier observed by Suter and co-workers due to a decoupling sequence being applied on environment spins [32].

Fig. 6.10 shows the comparison between the theoretical $S(\omega)$ using the methods given by Teklemariam *et al.* and Yuge *at el.* vs the experiemental $S(\omega)$ with

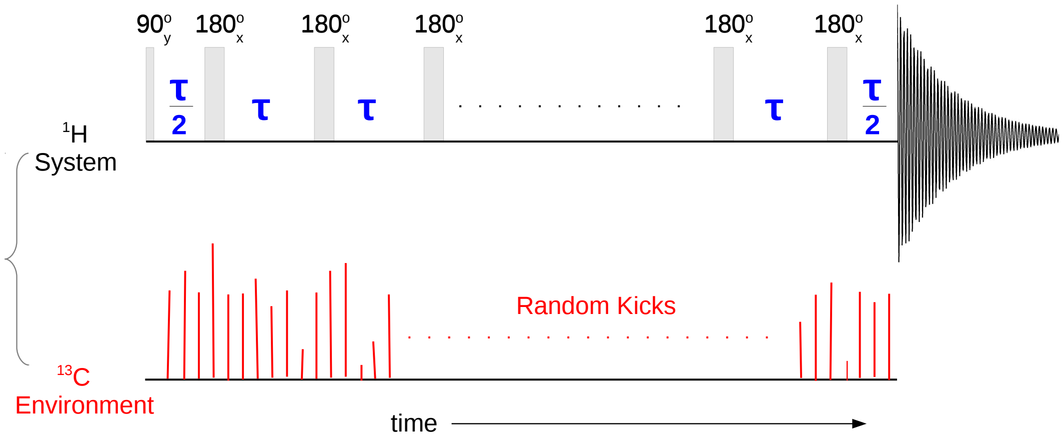

Figure 6.8: Measuring NS in the presence of kicks. The pulses on ^{1}H is basically CPMG sequence to measure T_2.

for kick-rate of 25 kicks/ms and kick-angles in the range 0 to 2 degrees. To obtain the experimental $S(\omega)$ due to kicks alone, we subtracted the intrinsic spectral density of the system qubit (with no kicks) from the total spectral density with kicks. A fair agreement between the numerically simulated curve and the experimental data confirms the relevance of the model in low Γ regime as given in [31].

We also characterized the induced phase decoherence by QPT and the general protocol was given in section 6.4.2. The single qubit QPT protocol consisted of the initial preparation of the four states as follows: $\rho_j = |\psi_j\rangle\langle\psi_j|$, with $|\psi_j\rangle \in \{|0\rangle, |1\rangle, (|0\rangle + |1\rangle)/\sqrt{2}, (|0\rangle - i|1\rangle)/\sqrt{2}\}$. The fixed set of operators as $\tilde{E}_p$ were chosen from the set $\{E, X, -iY, Z\}$, where E is the identity matrix and X, Y, Z are the Pauli matrices. The goal is to obtain the χ matrix which corresponds to kick induced noise process.

Fig. 6.11 shows the experimental QPT of the phase decoherence process for various kick parameters. The top figures correspond to the entire χ matrix expressed in the basis of $\{E, X, -iY, Z\}$. Among these figure are QPT of NOOP which is an Identity operator, i.e., no kicks and no DD, only kicks, UDD with

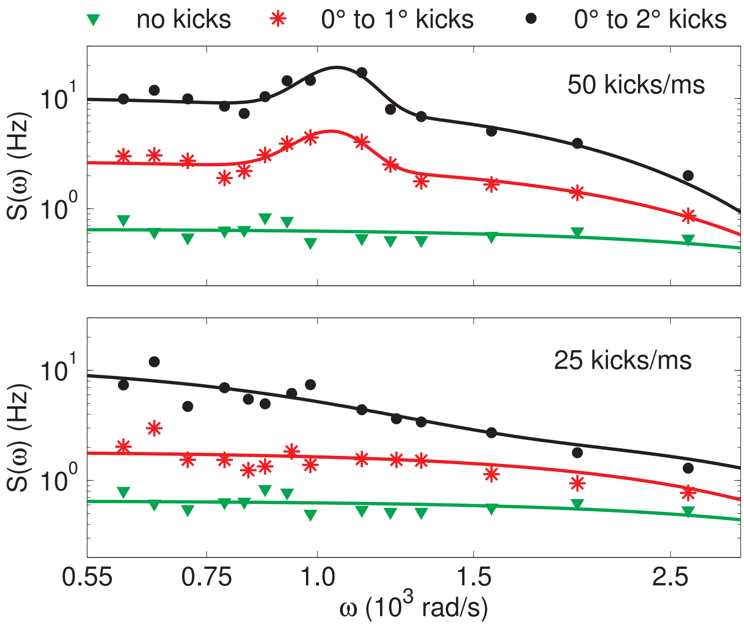

Figure 6.9

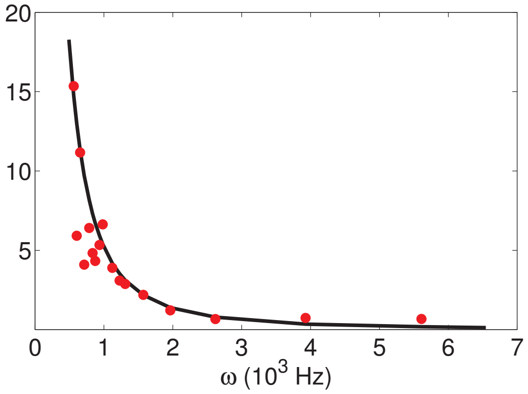

Figure 6.10: The experimental $S(\omega)$ (dots) vs the theoretical $S(\omega)$ (solid curve) corresponding to the kick parameters $\Gamma = 25$ kicks/ms and $\epsilon_m \in [0^\circ, 2^\circ]$.

kicks and CPMG DD with kicks. As evident, the Identity process has only EE component while the QPT in the presence of kicks has additional components in the χ matrix. As was already explained in section 6.2.1, the system-environment interaction of the type ZZ gives rise to phase decoherence which corresponds to ZZ components in the figure, thus indicating that the decoherence that we

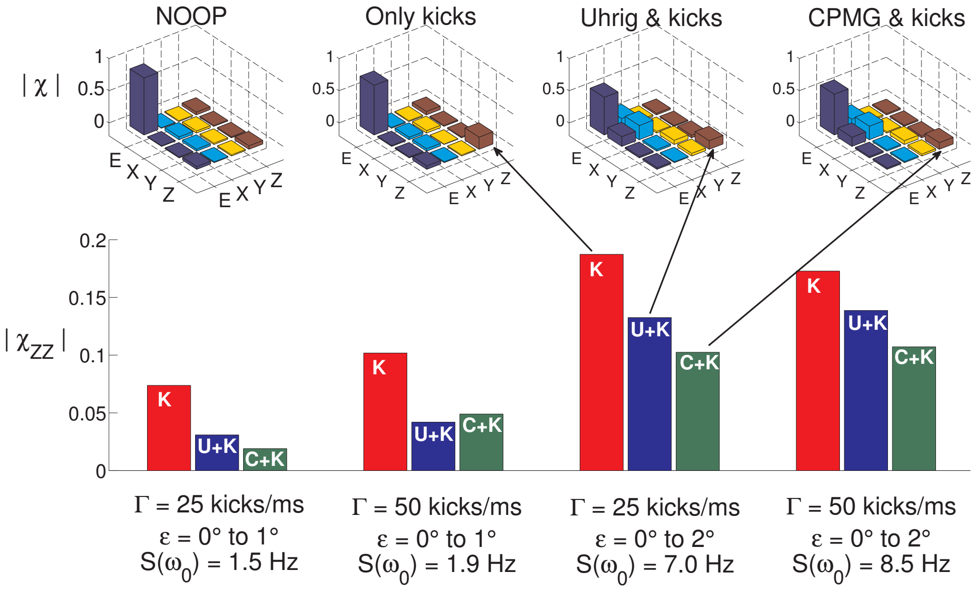

Figure 6.11

induced and studied was indeed phase decoherence. The extra components like EX, XE and XX arise due to the nonidealities in the π pulses in the DD sequences that introduce NOT operations.

6.6 Conclusion

Bibliography

[1] R. Feynman, “Simulating physics with computers,” *International Journal of Theoretical Physics*, vol. 21, no. 6-7, pp. 467–488, 1982.

[2] M. Planck, “On the law of distribution of energy in the normal spectrum,” *Annalen der Physik*, vol. 4, no. 553, p. 1, 1901.

[3] R. Shankar, *Principles of quantum mechanics*. Springer Science & Business Media, 2012.

[4] J. J. Sakurai and J. Napolitano, *Modern quantum mechanics*. Addison-Wesley, 2011.

[5] P. A. M. Dirac, *The principles of quantum mechanics*. Oxford university press, 1981, no. 27.

[6] M. A. Nielsen and I. L. Chuang, *Quantum computation and quantum information*. Cambridge university press, 2010.

[7] J. Preskill, “Lecture notes for physics 229: Quantum information and computation,” *California Institute of Technology*, 1998.

[8] D. P. DiVincenzo, “Quantum computation,” *Science*, vol. 270, no. 5234, pp. 255–261, 1995.

[9] D. DiVincenzo, “The physical implementation of quantum computation,” *arXiv preprint quant-ph/0002077*, 2000.

[10] I. Georgescu, S. Ashhab, and F. Nori, "Quantum simulation," *Reviews of Modern Physics*, vol. 86, no. 1, p. 153, 2014.

[11] C. Tseng, S. Somaroo, Y. Sharf, E. Knill, R. Laflamme, T. F. Havel, and D. G. Cory, "Quantum simulation of a three-body-interaction hamiltonian on an nmr quantum computer," *Physical Review A*, vol. 61, no. 1, p. 012302, 1999.

[12] S. S. Hegde, H. Katiyar, T. S. Mahesh, and A. Das, "Freezing a quantum magnet by repeated quantum interference: An experimental realization," *Physical Review B*, vol. 90, no. 17, p. 174407, 2014.

[13] S. S. Hegde, K. Rao, and T. S. Mahesh, "Pauli decomposition over commuting subsets: Applications in gate synthesis, state preparation, and quantum simulations," *arXiv preprint arXiv:1603.06867*, 2016.

[14] S. S. Hegde and T. S. Mahesh, "Engineered decoherence: Characterization and suppression," *Physical Review A*, vol. 89, no. 6, p. 062317, 2014.

[15] N. A. Gershenfeld and I. L. Chuang, "Bulk spin-resonance quantum computation," *science*, vol. 275, no. 5298, pp. 350–356, 1997.

[16] D. G. Cory, A. F. Fahmy, and T. F. Havel, "Ensemble quantum computing by nmr spectroscopy," *Proceedings of the National Academy of Sciences*, vol. 94, no. 5, pp. 1634–1639, 1997.

[17] D. Loss and D. P. DiVincenzo, "Quantum computation with quantum dots," *Physical Review A*, vol. 57, no. 1, p. 120, 1998.

[18] G. K. Brennen, C. M. Caves, P. S. Jessen, and I. H. Deutsch, "Quantum logic gates in optical lattices," *Physical Review Letters*, vol. 82, no. 5, p. 1060, 1999.

[19] J. I. Cirac and P. Zoller, "Quantum computations with cold trapped ions," *Physical review letters*, vol. 74, no. 20, p. 4091, 1995.

[20] J. Mooij, T. Orlando, L. Levitov, L. Tian, C. H. Van der Wal, and S. Lloyd, "Josephson persistent-current qubit," *Science*, vol. 285, no. 5430, pp. 1036–1039, 1999.

[21] X. Peng, J. Du, and D. Suter, "Quantum phase transition of ground-state entanglement in a heisenberg spin chain simulated in an nmr quantum computer," *Physical Review A*, vol. 71, no. 1, p. 012307, 2005.

[22] G. A. Álvarez and D. Suter, "Nmr quantum simulation of localization effects induced by decoherence," *Physical Review Letters*, vol. 104, no. 23, p. 230403, 2010.

[23] D. I. Tsomokos, S. Ashhab, and F. Nori, "Using superconducting qubit circuits to engineer exotic lattice systems," *Physical Review A*, vol. 82, no. 5, p. 052311, 2010.

[24] D. Porras and J. I. Cirac, "Quantum manipulation of trapped ions in two dimensional coulomb crystals," *Physical review letters*, vol. 96, no. 25, p. 250501, 2006.

[25] K. R. K. Rao, T. S. Mahesh, and A. Kumar, "Efficient simulation of unitary operators by combining two numerical algorithms: An nmr simulation of the mirror-inversion propagator of an x y spin chain," *Physical Review A*, vol. 90, no. 1, p. 012306, 2014.

[26] R. Shankar, S. S. Hegde, and T. S. Mahesh, "Quantum simulations of a particle in one-dimensional potentials using nmr," *Physics Letters A*, vol. 378, no. 1, pp. 10–15, 2014.

[27] V. S. Anjusha, S. S. Hegde, and T. S. Mahesh, "Nmr investigation of the quantum pigeonhole effect," *Physics Letters A*, vol. 380, no. 4, pp. 577 – 580, 2016.

[28] A. D. Greentree, C. Tahan, J. H. Cole, and L. C. Hollenberg, "Quantum phase transitions of light," *Nature Physics*, vol. 2, no. 12, pp. 856–861, 2006.

[29] M. Greiner, O. Mandel, T. Esslinger, T. W. Hänsch, and I. Bloch, "Quantum phase transition from a superfluid to a mott insulator in a gas of ultracold atoms," *nature*, vol. 415, no. 6867, pp. 39–44, 2002.

[30] A. Das, "Exotic freezing of response in a quantum many-body system," *Phys. Rev. B*, vol. 82, p. 172402, Nov 2010.

[31] G. Teklemariam, E. M. Fortunato, C. C. López, J. Emerson, J. P. Paz, T. F. Havel, and D. G. Cory, "Method for modeling decoherence on a quantum-information processor," *Phys. Rev. A*, vol. 67, p. 062316, Jun 2003.

[32] G. A. Álvarez and D. Suter, "Measuring the spectrum of colored noise by dynamical decoupling," *Phys. Rev. Lett.*, vol. 107, p. 230501, Nov 2011.

[33] T. Yuge, S. Sasaki, and Y. Hirayama, "Measurement of the noise spectrum using a multiple-pulse sequence," *Phys. Rev. Lett.*, vol. 107, p. 170504, Oct 2011.

[34] L. Landau, "Das dämpfungsproblem in der wellenmechanik," *Zeitschrift für Physik*, vol. 45, no. 5-6, pp. 430–441, 1927.

[35] D. H. Dunlap and V. M. Kenkre, "Dynamic localization of a charged particle moving under the influence of an electric field," *Phys. Rev. B*, vol. 34, pp. 3625–3633, Sep 1986.

[36] F. Grossmann, T. Dittrich, P. Jung, and P. Hänggi, "Coherent destruction of tunneling," *Phys. Rev. Lett.*, vol. 67, pp. 516–519, Jul 1991.

[37] J. Cavanagh, W. J. Fairbrother, A. G. Palmer III, and N. J. Skelton, *Protein NMR spectroscopy: principles and practice*. Academic Press, 1995.

[38] W. H. Zurek, S. Habib, and J. P. Paz, “Coherent states via decoherence,” *Physical Review Letters*, vol. 70, no. 9, p. 1187, 1993.

[39] J. Poyatos, J. Cirac, and P. Zoller, “Quantum reservoir engineering with laser cooled trapped ions,” *Physical review letters*, vol. 77, no. 23, p. 4728, 1996.

[40] C. J. Myatt, B. E. King, Q. A. Turchette, C. A. Sackett, D. Kielpinski, W. M. Itano, C. Monroe, and D. J. Wineland, “Decoherence of quantum superpositions through coupling to engineered reservoirs,” *Nature*, vol. 403, no. 6767, pp. 269–273, 2000.

[41] J. P. Paz and W. H. Zurek, “Quantum limit of decoherence: Environment induced superselection of energy eigenstates,” *Physical Review Letters*, vol. 82, no. 26, p. 5181, 1999.

[42] J. P. Paz, “Quantum engineering: protecting the quantum world,” *Nature*, vol. 412, no. 6850, pp. 869–870, 2001.

[43] L. Viola and S. Lloyd, “Dynamical suppression of decoherence in two-state quantum systems,” *Phys. Rev. A*, vol. 58, pp. 2733–2744, Oct 1998. [Online]. Available: http://link.aps.org/doi/10.1103/PhysRevA.58.2733

[44] W. H. Zurek, “Environment-induced superselection rules,” *Physical Review D*, vol. 26, no. 8, p. 1862, 1982.

[45] S. Meiboom and D. Gill, “Modified spin-echo method for measuring nuclear relaxation times,” *Review of scientific instruments*, vol. 29, no. 8, pp. 688–691, 1958.

[46] G. S. Uhrig, “Keeping a quantum bit alive by optimized π-pulse sequences,” *Physical Review Letters*, vol. 98, no. 10, p. 100504, 2007.

[47] J. Preskill, “Reliable quantum computers,” in *Proceedings of the Royal Society of London A: Mathematical, Physical and Engineering Sciences*, vol. 454, no. 1969. The Royal Society, 1998, pp. 385–410.

[48] E. Farhi, J. Goldstone, S. Gutmann, and M. Sipser, “Quantum computation by adiabatic evolution,” *arXiv preprint quant-ph/0001106*, 2000.

[49] D. A. Lidar and K. B. Whaley, “Decoherence-free subspaces and subsystems,” in *Irreversible Quantum Dynamics*. Springer, 2003, pp. 83–120.

[50] H. K. Ng, D. A. Lidar, and J. Preskill, “Combining dynamical decoupling with fault-tolerant quantum computation,” *Physical Review A*, vol. 84, no. 1, p. 012305, 2011.

[51] J. Zhang, A. M. Souza, F. D. Brandao, and D. Suter, “Protected quantum computing: interleaving gate operations with dynamical decoupling sequences,” *Physical review letters*, vol. 112, no. 5, p. 050502, 2014.

[52] E. L. Hahn, “Spin echoes,” *Physical review*, vol. 80, no. 4, p. 580, 1950.

[53] M. J. Biercuk, H. Uys, A. P. VanDevender, N. Shiga, W. M. Itano, and J. J. Bollinger, “Optimized dynamical decoupling in a model quantum memory,” *Nature*, vol. 458, no. 7241, pp. 996–1000, 2009.

[54] M. Biercuk, A. Doherty, and H. Uys, “Dynamical decoupling sequence construction as a filter-design problem,” *Journal of Physics B: Atomic, Molecular and Optical Physics*, vol. 44, no. 15, p. 154002, 2011.

[55] Y. Pan, Z.-R. Xi, and J. Gong, “Optimized dynamical decoupling sequences in protecting two-qubit states,” *Journal of Physics B: Atomic, Molecular and Optical Physics*, vol. 44, no. 17, p. 175501, 2011.

[56] I. L. Chuang and M. A. Nielsen, “Prescription for experimental determination of the dynamics of a quantum black box,” *Journal of Modern Optics*, vol. 44, no. 11-12, pp. 2455–2467, 1997.

[57] K. Vogel and H. Risken, “Determination of quasiprobability distributions in terms of probability distributions for the rotated quadrature phase,” *Phys. Rev. A*, vol. 40, pp. 2847–2849, Sep 1989.

[58] U. Leonhardt, *Measuring the quantum state of light*. Cambridge university press, 1997, vol. 22.

[59] A. Ajoy, G. A. Álvarez, and D. Suter, “Optimal pulse spacing for dynamical decoupling in the presence of a purely dephasing spin bath,” *Phys. Rev. A*, vol. 83, p. 032303, Mar 2011. [Online]. Available: http://link.aps.org/doi/10.1103/PhysRevA.83.032303

[60] S. S. Roy, T. S. Mahesh, and G. S. Agarwal, “Storing entanglement of nuclear spins via uhrig dynamical decoupling,” *Phys. Rev. A*, vol. 83, p. 062326, Jun 2011. [Online]. Available: http://link.aps.org/doi/10.1103/PhysRevA.83.062326

[61] B. Cowan, *Nuclear magnetic resonance and relaxation*. Cambridge University Press, 2005.